CONF-800787--1

HADRON NUCLEUS INTERACTIONS

H. Feshbach

Center for Theoretical Physics
Laboratory for Nuclear Science and Department of Physics
Massachusetts Institute of Technology
Cambridge, MA 02139

MASTER

Presented at the International School of Physics "Enrico Fermi"
Varenna, Lake Como, Italy, July 1980.

This work is supported in part through funds provided by the
U.S. Department of Energy (DOE) under contract OE-AC02-76ERO-3069.

October 1980
CTP #894

DISCLAIMER

This book was prepared as an account of work sponsored by an agency of the United States Government. Neither the United States Government nor any agency thereof, nor any of their employees, makes any warranty, express or implied, or assumes any legal liability or responsibility for the accuracy, completeness, or usefulness of any information, apparatus, product, or process disclosed, or represents that its use would not infringe privately owned rights. Reference herein to any specific commercial product, process, or service by trade name, trademark, manufacturer, or otherwise, does not necessarily constitute or imply its endorsement, recommendation, or favoring by the United States Government or any agency thereof. The views and opinions of authors expressed herein do not necessarily state or reflect those of the United States Government or any agency thereof.

H. FESHBACH

Department of Physics
Massachusetts Institute of Technology
Cambridge, Massachusetts 02139

I. Introduction

It is, of course, not possible in four lectures to present a complete survey of the many aspects of the interaction of energetic hadrons with nuclei. I have therefore selected a number of topics which suffice to illustrate the wide range of phenomena of interest, that at the same time involve issues of central importance that can be addressed using broadly applicable theoretical methods. The first lecture will consider the elastic and inelastic scattering of intermediate energy ($\gtrsim$ 1 GeV) protons by nuclei. The discussion will focus on the determination of the proton-nucleus optical potential in terms of the elementary nucleon-nucleon scattering amplitudes and the properties of the target and residual nucleus. The result will be a series of terms for the optical potential of which we will evaluate the first two illustrated in Fig. (1.1) for the case of elastic scattering. In Fig. (1.1a) the nucleon-nucleon interaction, indicated by a broken line, acts once, the target nucleus remaining in its ground state. In Fig. (1.1b) the target nucleus is excited by the first interaction returning to its ground state as a result of the second interaction. If inelastic scattering to a particular final state is under consideration, diagrams in which the target nucleus can also return to that state in

DISTRIBUTION OF THIS DOCUMENT IS UNLIMITED

the final step of Fig. (1.1a) and Fig. (1.1b) should be included. Hence in inelastic scattering there are four diagrams according to whether the target returns to the ground or excited state. The optical potential these represent are suitably iterated by the Schroedinger equation to produce the elastic and *inelastic amplitudes.*

The approximation used to evaluate the potential corresponding to Fig. (1.1b) is referred to as the closure approximation. It assumes first that the intermediate excited target states which contribute substantially have energies which are small compared to the incident energy, and second that among these there are no specially important states which would need correspondingly special consideration. Our application of this formalism, referred to as the multiple scattering approximation, will be made to proton-nuclear scattering for protons whose energies are of the order of 1 GeV. However, the same procedure should be equally valid for sufficiently energetic hadrons generally.

The second topic to be considered in these lectures is the interaction of pions with nuclei for energies in the neighborhood of the Δ-resonance. In this energy domain an incident pion will with high probability be absorbed by a nucleon, producing the Δ-resonance and forming thereby a Δ-particle hole state in the nucleus. In this case, the closure approximation of multiple scattering theory is not valid for, as we shall see, the Δ-particle hole state can act as a doorway state having a particularly large overlap with the incident channel. This mechanism proposed by Kisslinger and Wang and developed by Lenz and Moniz and their collaborators is known as the "Isobar Doorway" model. From the consequent analysis we have an insight into the impact of the nuclear environment on the properties of the Δ inside nuclei and how it depends upon the nature of that environment. It is clear that this analysis can be *used to discuss the behavior of other baryonic resonances such as the Y* inside* nuclei and their use as probes of nuclear properties.

The stable baryons can be used as probes. The Λ hypernuclei (consisting of a core nucleus and a Λ) and the recently observed Σ hypernuclei provide us with situations in which the core nucleus can be probed by a baryon of roughly the same mass as a nucleon, with similar albeit not identical interactions with nucleons. But, and this is an important point, the Λ (or Σ) does not need to satisfy the Pauli exclusion principle with respect to the nucleons and therefore can be in orbits forbidden to it if it were a nucleon. This subject of hypernuclei will be the third topic taken up in these lectures.

As the energy of the projectile increases, it becomes correspondingly more important to take relativistic effects into account. The importance of these effects is strikingly revealed by experiments involving the collision of ultra-relativistic hadrons, protons, pions, kaons (up to Fermilab energies) with nuclei. This phenomenon will form part of the fourth topic which will include as well the collision of relativistic heavy ion projectiles with nuclei. A nuclear Weiszäcker-Williams method developed for dealing with peripheral collisions will be described.

II. Proton-Nuclear Scattering in the Multiple Scattering Approximation [1,2]

Formally the theory of multiple scattering attempts to solve the following problem. Let the potential acting between the incident projectile and the nucleus be given by a sum of two-body potentials:

$$\sum_i v_i \mathcal{A} \tag{2.1}$$

where v_i is the potential acting between the incident particle and the i'th nucleon of the target nucleus. $\mathcal{A}$ is the anti-symmetrization projection operator limiting the action of the interaction to the Hilbert space formed by anti-symmetric wave functions describing various states of the target nucleus. The interaction given by Eq. (2.1) is non-relativistic. The only relativistic

effects which are explicitly included in the theory to be described below are primarily kinematic in nature, taking into account the variation of mass with energy.* Since the potential description is used, effects of the virtual boson fields, nucleon isobars, etc. are not completely included. However, the formalism can be extended to take these additional degrees of freedom into account.

Two methods have been used to solve the scattering generated by the interaction given by Eq. (2.1). We shall limit the discussion here to that developed by Watson [3] and by Kerman, McManus and Thaler [1]. The other associated with Glauber [4] is described in many texts [5].

The Lippman-Schwinger equation for the transition matrix $\mathcal{J}$ is given by

$$\mathcal{J} = \sum_{1}^{N} v_i a + \sum_{1}^{N} v_i \frac{a}{\alpha} \mathcal{J} \tag{2.2}$$

where

$\alpha = E^{(+)} - K - H_N$

H_N = target Hamiltonian

K = the kinetic energy operation for the incident projectile relative to the center of mass of the target nucleus

N = number of nucleons in the target nucleus.

Our goal is to relate $\mathcal{J}$ and the two body scattering transition amplitude describing the scattering of the incident projectile by a free nucleon. The Lippman-Schwinger equation for that transition matrix describing the scattering from the i'th nucleon is

$$t_i = v_i + v_i \frac{1}{E^{(+)} - K_0} t_i \tag{2.4}$$

where K_0 is the kinetic energy operator for the incident projectile relative

* A Klein-Gordon equation is used with the optical potential being treated as the fourth component of a four vector.

to the i'th nucleon.

As an intermediate step, KMT introduce the many-body operator τ defined by:

$$\tau = \frac{1}{N} \sum v_i a + \frac{1}{N} \sum v_i \frac{a}{\alpha} \tau \tag{2.5}$$

Very roughly, τ is given by t_i averaged over the scatterers. A precise relation between τ and t_i will be given later. Eq. (2.5) can be used to eliminate v_i in the equation for $\mathcal{J}$. Writing

$$\sum v_i a = \left(N - \sum v_i \frac{a}{\alpha}\right)\tau$$

and noting that

$$\tau \frac{1}{\alpha} \sum v_i a = \sum v_i \frac{a}{\alpha} \tau$$

substitution in Eq. (2.2) yields

$$\mathcal{J} = \left(N - \sum v_i \frac{a}{\alpha}\right)\tau + \left(N - \sum v_i \frac{a}{\alpha}\right)\tau \frac{1}{\alpha} \mathcal{J}$$

or

$$\mathcal{J} = N\tau + N\tau \frac{1}{\alpha} \mathcal{J} - \tau \frac{1}{\alpha}\left(\sum v_i a + \sum v_i a \frac{1}{\alpha} \mathcal{J}\right)$$

Using Eq. (2.2) again, one obtains $\mathcal{J}$ in terms of τ:

$$\mathcal{J} = N\tau + (N-1)\tau \frac{1}{\alpha} \mathcal{J} \tag{2.6}$$

Let

$$\mathcal{J} = \frac{N}{N-1} \mathcal{J}' \tag{2.7}$$

Then

$$\mathcal{J}' = (N-1)\tau + (N-1)\tau \frac{1}{\alpha} \mathcal{J}' \tag{2.8}$$

This is just a Lippman-Schwinger equation where the interaction is an effective one being given not by a sum of two body operators v_i but by the many-body operator τ. The principal advantage of this transformation is that τ is more clearly related to t_i than v_i. In the following we shall obtain a Schroedinger equation whose transition amplitude is $\mathcal{J}'$. To obtain that result will need to be multiplied by N/N-1.

One can rewrite Eq. (2.8) as a Schroedinger equation for the wave function of the system Ψ:

$$(E - K - \tilde{H}_N - (N-1)\tau)\,\Psi = 0 \tag{2.9}$$

We now proceed to derive the optical model potential. Two possible forms will be obtained. One in which we are concerned with only a single channel, the elastic. A second form pertains to a two channel situation, an elastic channel and say one inelastic channel. In this case the optical potential becomes a two by two matrix, the non-diagonal components coupling the elastic and inelastic channels. It is easy to generalize the results to include several inelastic channels. Let P be a projection operator which projects Ψ onto these reaction channels, the elastic and the inelastic one of interest. Explicitly

$$P\Psi = |0\rangle\langle 0|\Psi + |1\rangle\langle 1|\Psi \tag{2.10}$$

where $|0\rangle$ and $|1\rangle$ are the state vectors for the ground and excited state respectively. Let the complementary projection operator be Q so that

$$Q = 1 - P \;,\quad PQ = 0 \;,\quad P^2 = P \;,\quad Q^2 = Q \tag{2.11}$$

Introducing the notation

$$\tau_{PP} = P\tau P, \quad \tau_{PQ} = P\tau Q$$

one can rewrite Eq. (2.9) as follows:

$$[E - K - (H_N)_{PP} - (N-1)\tau_{PP}](P\Psi) = (N-1)\tau_{PQ}(Q\Psi) \tag{2.12a}$$

$$[E - K - (H_N)_{QQ} - (N-1)\tau_{QQ}](Q\Psi) = (N-1)\tau_{QP}(P\Psi) \tag{2.12b}$$

Solving the second equation for $Q\Psi$ and substituting in Eq. (2.12a) yields

$$\left[E - K - (H_N)_{PP} - \tau_{PP} - (N-1)^2\tau_{PQ}\frac{1}{E^{(+)} - K - (H_N)_{QQ} - (N-1)\tau_{QQ}}\tau_{QP}\right]P\Psi = 0 \tag{2.13}$$

The effective optical potential is given by the terms in τ in this equation. So far no approximations have been made. We shall however eventually neglect the effect of the Pauli exclusion principle when the incident projectile contains nucleons. In that case the error for forward scattering amplitude is small. (See Watson and Takeda [6] for discussion.) A second approximation to be employed below and to which we referred in the introduction as the closure approximation involves replacing $(N-1)\tau_{QQ}$ by an average potential $\bar{V}$ and $(H_N)_{QQ}$ by an average energy $\bar{\varepsilon}$. Under these circumstances, the propagator in the last term in the square bracket in Eq. (2.13) is diagonal in the coordinates of the target nucleus. In this approximation, the "closure approximation," any explicit reference to the states in the Hilbert space projected by Q disappears.

To obtain an optical potential in terms of t_i it is necessary to relate τ and t_i. Toward this end define the operators τ_i:

$$\tau = a\tau_i = \frac{1}{N}\sum \tau_i \tag{2.14}$$

Comparing with Eq. (2.5) we have

$$\tau_i = v_i a + v_i \frac{a}{\alpha}\tau \tag{2.15}$$

Rather than dealing immediately with t_i we define t_i' to which t_i will reduce in the limit of high energies.

$$t_i' = v_i + v_i \frac{1}{\alpha} t_i' \tag{2.16}$$

We may eliminate v_i between these last two equations using a method identical to that which led from Eq. (2.2) to Eq. (2.6). The result is

$$\tau = \frac{1}{N}\sum t_i' \mathcal{A} + \frac{1}{N}\sum t_i' \frac{\mathcal{A}-1}{\alpha} \tau_i \tag{2.17}$$

In order to insert this result into the optical potential it is most convenient to replace $(1/\alpha)$ by $(1/\tilde{\alpha})$ where

$$\tilde{\alpha} \equiv E^{(+)} - K - H_N - (N-1)\tau$$

Comparing $(1/\alpha)$ and $(1/\tilde{\alpha})$ one obtains

$$\frac{1}{\alpha} = \frac{1}{\tilde{\alpha}} - \frac{1}{\tilde{\alpha}}(N-1)\tau\frac{1}{\alpha}$$

But then the rather remarkable result follows:

$$\frac{\mathcal{A}-1}{\alpha} = \frac{\mathcal{A}-1}{\tilde{\alpha}}$$

since $(\mathcal{A}-1)\mathcal{A} = 0$. Hence in Eq. (2.17) one can replace α by $\tilde{\alpha}$. To the second order of approximation (in t') Eq. (2.17) becomes

$$\tau \simeq \frac{1}{N}\sum t_i' \mathcal{A} + \frac{1}{N}\sum t_i' \frac{\mathcal{A}-1}{\tilde{\alpha}} t_i' \tag{2.18}$$

It is important to realize that the second term has as one of its functions guaranteeing that the final result takes proper account of the Pauli principle for the target nucleons.

It is inconvenient to continue to carry the operator $\mathcal{A}$. Since $(1/N)\Sigma t_i'$ is a symmetric operator, the $\mathcal{A}$ in the first term is superfluous. Hence the operator $(N-1)\tau$ is approximately given by

$$(N-1)\tau = (N-1)\left\{\frac{1}{N}\sum_i t_i' + \frac{1}{N^2}\sum t_i' \frac{1}{\tilde{\alpha}}\sum t_j' - \frac{1}{N}\sum t_i' \frac{1}{\tilde{\alpha}} t_i'\right\} \tag{2.19}$$

Returning to Eq. (2.13), replacing τ by expression Eq. (2.19), replacing $(N-1)\tau_{QQ}$ by $\bar{V}$ and $(H_N)_{QQ}$ by $\bar{\varepsilon}$ as described above, and keeping only terms which

are bilinear in t_i' yields after some calculation

$$V_{OPT} \simeq \frac{N-1}{N}\sum t_i' + \frac{N-1}{N}\sum_{i\neq j} t_i' \frac{1}{\tilde{\alpha}} t_j' - \frac{(N-1)^2}{N^2}\sum_i t_i' \frac{\mathcal{P}}{\tilde{\alpha}}\sum_j t_j' \tag{2.20}$$

At this point we shall replace t_i' by t_i. Comparison of Eq. (2.16) with (2.4) permits the calculation of a correction for this approximation.

We now consider two situations. The first is elastic scattering.

(a) Elastic Scattering

For this case $\mathcal{P}$ projects only on the elastic channel. Consider the first term in Eq. (2.20) in the momentum representation:

$$V_{OPT}^{(1)}(\vec{k},\vec{k}') = \frac{N-1}{N}\langle 0,\vec{k}|\sum t_i|0,\vec{k}'\rangle \tag{2.21}$$

where the state vector describing the target nucleus in the ground state and the projectile state one of momentum $\vec{k}'$ is $|0\vec{k}'\rangle$. Because of the second term in Eq. (2.4), t_i is generally a non-local operator:

$$t_i = t(\vec{r}_0-\vec{r}_i, \vec{r}_0'-\vec{r}_i')\,\delta\left(\tfrac{1}{2}(\vec{r}_0+\vec{r}_i) - \tfrac{1}{2}(\vec{r}_0'+\vec{r}_i')\right)$$

where $\vec{r}_0$ and $\vec{r}_0'$ are the coordinates of the projectile, $\vec{r}_i$ and $\vec{r}_i'$ the coordinates of the target nucleon with which it interacts. $V_{OPT}^{(1)}$ can then be written

$$V_{OPT}^{(1)} = \frac{N-1}{N}\sum_i \int d\vec{r}_0' \int d\vec{r}_0 \int d\vec{r}_i \int d\vec{r}_i'\, \rho^{(1)}(\vec{r}_i,\vec{r}_i')\, e^{-i\vec{k}\cdot\vec{r}_0} \times t(\vec{r}_0-\vec{r}_i, \vec{r}_0'-\vec{r}_i')\,\delta\left(\tfrac{1}{2}(\vec{r}_0+\vec{r}_i) - \tfrac{1}{2}(\vec{r}_0'+\vec{r}_i')\right) e^{i\vec{k}'\cdot\vec{r}_0'} \tag{2.22}$$

where $\rho^{(1)}$ is the density matrix:

$$\rho^{(1)}(\vec{r}_i,\vec{r}_i') = \int \psi_0^*(\vec{r}_1,\ldots,\vec{r}_{i-1},\vec{r}_i,\vec{r}_{i+1},\ldots)\,\psi_0(\vec{r}_1,\ldots,\vec{r}_{i-1},\vec{r}_i',\vec{r}_{i+1},\ldots) \times d\vec{r}_1\ldots d\vec{r}_{i-1}\, d\vec{r}_{i+1}\ldots \tag{2.23}$$

We briefly summarize the steps taken to evaluate Eq. (2.22). It is convenient to introduce the Fourier transform of $\rho^{(1)}$:

$$\rho^{(1)}(\vec{r}_i,\vec{r}_i') = \frac{1}{(2\pi)^6}\iint e^{i\vec{q}\cdot\vec{r}_i - i\vec{q}'\cdot\vec{r}_i'}\,\tilde{\rho}(\vec{q},\vec{q}')\,d\vec{q}\,d\vec{q}' \tag{2.24}$$

and the relative and center of mass variables $\vec{r} = \vec{r}_0 - \vec{r}_j$ and $\vec{R} = \frac{1}{2}(\vec{r}_0 + \vec{r}_j)$ together with similar coordinates for the primed variables. The calculation is straightforward leading to

$$V^{(1)}_{OPT}(\vec{k},\vec{k}') = (N-1)\left(\frac{1}{2\pi}\right)^6 \int d\vec{q} \int d\vec{q}'\, \bar{\rho}(\vec{q},\vec{q}')\, t\left(\frac{\vec{q}+\vec{k}}{2}, \frac{\vec{q}'+\vec{k}'}{2}\right) \times \delta(\vec{q}-\vec{k}-(\vec{q}'-\vec{k}')) \tag{2.25}$$

where

$$t(\vec{x},\vec{x}') = \iint e^{-i\vec{x}\cdot\vec{p} + i\vec{x}'\cdot\vec{p}'}\, t(\vec{p},\vec{p}')\, d\vec{p}\, d\vec{p}' \tag{2.26}$$

The physical interpretation of Eq. (2.25) is straightforward. The projectile provides a momentum $\vec{k}'$ the target $\vec{q}'$. After the collision the projectile has a momentum k and the target $\vec{q}$. The delta function guarantees that the momentum transferred to the target, $\vec{q} - \vec{q}'$, equals the momentum lost by the projectile $\vec{k} - \vec{k}'$.

To obtain the familiar Rayleigh-Lax expression, we assume that

$$t(\vec{x},\vec{x}') = t(\vec{x}-\vec{x}') \tag{2.27}$$

One then obtains the result

$$V^{(1)}_{OPT}(\vec{k},\vec{k}') \simeq (N-1)\rho(\vec{k}'-\vec{k})\, t_E(\vec{k}-\vec{k}') \equiv V_{RL} \tag{2.28}$$

where

$$\rho(\vec{k}'-\vec{k}) = \int e^{i(\vec{k}'-\vec{k})\cdot\vec{r}}\, \rho(\vec{r})\, d\vec{r} \tag{2.29}$$

and

$$\rho(\vec{r}) \equiv \rho^{(1)}(\vec{r},\vec{r}) \tag{2.30}$$

In Eq. (2.28) we have made the energy dependence of $t_E(\vec{k} - \vec{k}')$ explicit. This amplitude is in fact the full off-energy shell t matrix. Thus more than the empirical values of the projectile-nucleon scattering which provides only the

on-shell amplitudes is required. In fact, the complete characterization of the projectile-nucleon interaction is needed. In practice, one has proceeded by fitting the nucleon-projectile transition amplitude on the energy shell, generally using a function of $\vec{k} - \vec{k}'$ employing parameters which are allowed to vary with E. This form is then used to calculate the off-energy shell values required by Eq. (2.28). A typical form is

$$A(E)\, e^{-\beta(E)(\vec{k}-\vec{k}')^2}$$

We now turn to the next approximation constructed from the last two terms on the right hand side of Eq. (2.20). In making this calculation we shall immediately make approximations Eq. (2.26) and the equivalent of Eq. (2.27):

$$\rho^{(2)}(\vec{r}_i,\vec{r}_j;\vec{r}_i',\vec{r}_j') = \delta(\vec{r}_i-\vec{r}_i')\,\delta(\vec{r}_j-\vec{r}_j')\,\bar{\rho}^{(2)}(\vec{r}_i,\vec{r}_j) \tag{2.31}$$

where

$$\rho^{(2)} = \int \psi_0^*(\vec{r}_1 \ldots \vec{r}_i, \vec{r}_{i+1} \ldots \vec{r}_j \ldots)\, \psi_0(\vec{r}_1 \ldots \vec{r}_i', \vec{r}_{i+1} \ldots \vec{r}_j' \ldots)\, d\vec{r}_1 \ldots d\vec{r}_{i-1}\, d\vec{r}_{i+1} \ldots$$

and

$$\bar{\rho}^{(2)}(\vec{x},\vec{y}) = \frac{1}{N(N-1)} \sum_{i \neq j} \langle 0 | \delta(\vec{x}-\vec{r}_i)\,\delta(\vec{y}-\vec{r}_j) | 0 \rangle \tag{2.32}$$

while

$$\bar{\rho}^{2}(\vec{q},\vec{q}') = \int \bar{\rho}^{(2)}(\vec{x},\vec{y})\, \exp i(\vec{q}\cdot\vec{x} + \vec{q}'\cdot\vec{y})\, d\vec{x}\, d\vec{y} \tag{2.33}$$

We give the final result for the second order terms:

$$\begin{aligned} V^{(2)}_{OPT} &= \langle o\vec{k} | \text{second order} | o\vec{k}' \rangle \\ &= (N-1)^2 \int d\vec{k}'' \int d\vec{k}''\, t(\vec{k}''-\vec{k}) \langle \vec{k}'' | \frac{1}{\tilde{\alpha}} | \vec{k}''' \rangle\, t(\vec{k}'-\vec{k}''') \\ &\quad \times C^{(2)}(\vec{k}''-\vec{k},\ \vec{k}'-\vec{k}''') \end{aligned} \tag{2.34}$$

where $C^{(2)}$ the second order correlation* is defined by

$$C^{(2)}(\vec{q},\vec{q}\,') = \bar{\rho}^{(2)}(\vec{q},\vec{q}\,') - \rho(\vec{q})\rho(\vec{q}\,') \tag{2.35}$$

The third order contribution has been calculated by Ullo. As one might expect the third order correlation function occurs but in contrast with the second order term given above there are additional terms which depend upon ρ and $\rho^{(2)}$ which are of importance for light target nuclei.

(a') A Local Approximation

The potential $V^{(2)}_{OPT}$ is non-local, making its use in the Schroedinger equation comparatively difficult, albeit with modern computers possible. An approximate method which replaces the Schroedinger equation with the non-local potential by a pair of coupled Schroedinger equations involving only local potentials has been developed [2]. We shall only quote the results. The equations have the form:

$$\begin{aligned}(E-K-V_{RL})\psi &= A\psi^{(1)}\\ (E-\bar{\epsilon}-K-V_{RL})\psi^{(1)} &= A\psi\end{aligned} \tag{2.36}$$

As one can see from this equation, $\psi^{(1)}$ plays the role of an effective intermediate inelastic state. The construction of the coupling potential involves the following steps.

Let

$$X(\vec{q},\vec{q}\,') \equiv t(\vec{q})\,C^{(2)}(\vec{q},\vec{q}\,')\,t(\vec{q}\,') \tag{2.37}$$

*If approximation Eq. (2.31) and Eq. (2.26) are not made $C^{(2)}$ is replaced by

$$\rho^{(2)}(\vec{k},\vec{k}'';\vec{k}''',\vec{k}') - \bar{\rho}^{(1)}(\vec{k},\vec{k}'')\,\bar{\rho}^{(1)}(\vec{k}''',\vec{k}')$$

while the t's are replaced by the more accurate $t(\vec{k},\vec{k}'';E)$ and $t(\vec{k}''',\vec{k}';E)$ respectively.

and its Fourier transform:

$$\tilde{X}(\vec{r},\vec{r}\,') = \frac{1}{(2\pi)^6}\int d\vec{q}\int d\vec{q}\,'\,X(\vec{q},\vec{q}\,')\,\exp -i(\vec{q}\cdot\vec{r}+\vec{q}\,'\cdot\vec{r}\,') \tag{2.38}$$

Taking the z direction to be that of the vector $\vec{k}+\vec{k}'$, and denoting the perpendicular direction by $\vec{t}$, let

$$\begin{aligned}f^2(t^2) &= \int dz\int dz'\,\tilde{X}(\vec{t},z;\vec{t},z')\\ &= \frac{1}{(2\pi)^2}\int d\vec{Q}\,x(\vec{Q})\,e^{-2i\vec{Q}\cdot\vec{t}}\end{aligned} \tag{2.39}$$

where

$$\vec{Q} = \frac{1}{2}(\vec{q}+\vec{q}\,')$$

and

$$x(\vec{Q}) = \frac{1}{(2\pi)^2}\int d\vec{Q}'\,X(\vec{q}_\perp,0;\vec{q}\,'_\perp,0)$$

where

$$\vec{Q}' = \vec{q}_\perp - \vec{q}\,'_\perp$$

With these definitions the coupling potential is given by

$$A(r) = -\frac{1}{\pi}\int_{-\infty}^{\infty} f'(r^2+u^2)\,du \tag{2.40}$$

One advantage of this procedure is that it avoids the common practice of neglecting the longitudinal momentum transfer which would limit applicability to small angle scattering.

(a'') Spin Effects

The above discussion for $V^{(2)}$ is valid only when t is spin independent. This is of course not the case when the incident projectile is a nucleon. The necessary generalizations have been carried out by Lambert [2] and recently by Parmentola. We shall not describe their results here. Instead, a simpler

analysis appropriate when the nucleus can be described by LS coupling will be presented.

The nucleon-nucleon t matrix has the following form

$$t_i = A + B\vec{\sigma}_0\cdot\vec{\sigma}_i + C(\vec{\sigma}_0+\vec{\sigma}_i)\cdot\vec{n} + D\vec{\sigma}_0\cdot\vec{Q}\,\vec{\sigma}_i\cdot\vec{Q} + E\vec{\sigma}_0\cdot\vec{q}\,\vec{\sigma}_i\cdot\vec{q} \tag{2.41}$$

where $\vec{\sigma}_0$ and $\vec{\sigma}_i$ are the Pauli spin-operaturs for the projectile and target nucleus nucleon respectively. The vectors $\vec{n}$, $\vec{Q}$ and $\vec{q}$ are

$$\vec{q} \equiv \vec{k}-\vec{k}' \qquad Q \equiv \tfrac{1}{2}(\vec{k}+\vec{k}'), \qquad \vec{n} = (\vec{k}\times\vec{k}') \tag{2.42}$$

In evaluating the first term in Eq. (2.30), the Rayleigh-Lax term, one takes the expectation value with respect to the target nucleus. If that nucleus has zero spin the result as far as the spin operators are concerned is

$$A + C\,\vec{\sigma}_0\cdot\vec{n}$$

All other expectation values vanish. This result translates into a central plus a spin-orbit optical potential, a result which can be anticipated from invariance principles. The physical reason for the absence of any contribution from the other terms can be readily formulated. Roughly speaking, a term like $B\vec{\sigma}_0\cdot\vec{\sigma}_i$ results in a spin flip of the target nucleus nucleon, changing the state of the target nucleus. In order to restore the spin orientation a second scattering is necessary. Thus the B, D and E terms in Eq. (2.41) will contribute to $V^{(2)}_{OPT}$ and not to V_{RL}. Since the relatively small energy change involved in the spin flip can be neglected, it is clear that $V^{(2)}$ will be bilinear in the density in addition to its expected dependence on the second order correlation. It is useful to combine these density dependent terms with the first order term, Eq. (2.30), so that the remainder will depend only upon the correlation. As we shall see this can be done relatively easily.

Only a simple example will be discussed. Suppose t_i has the form:

$$t_i = t^{(0)} + \vec{\sigma}_0\cdot\vec{\sigma}_i\, t^{(1)} \tag{2.43}$$

Then

$$\langle 0\vec{k}|V_{RL}|0\vec{k}'\rangle = (N-1)\,t^{(0)}\rho \tag{2.44}$$

The calculation of $V^{(2)}_{OPT}$ will involve the evaluation of the quantity:

$$M(\vec{q},\vec{q}') \equiv \frac{1}{N(N-1)}\sum_{i\neq j}\langle 0|[t^{(0)}(\vec{q}) + \vec{\sigma}_0\cdot\vec{\sigma}_i\, t^{(1)}(\vec{q})][t^{(0)}(\vec{q}') + \vec{\sigma}_0\cdot\vec{\sigma}_j\, t^{(1)}(\vec{q}')]|0\rangle \tag{2.45}$$
$$- \rho(\vec{q})\rho(\vec{q}')\,t^{(0)}(\vec{q})\,t^{(0)}(\vec{q}')$$

Doing the spin algebra one obtains:

$$M(\vec{q},\vec{q}') = t^{(0)}(\vec{q})\,t^{(0)}(\vec{q}')\,C^{(2)}(\vec{q},\vec{q}')$$
$$+ t^{(1)}(\vec{q})\,t^{(1)}(\vec{q}')\frac{1}{N(N-1)}\sum_{i\neq j}\langle 0|\vec{\sigma}_i\cdot\vec{\sigma}_j\, e^{i(\vec{q}\cdot\vec{r}_i+\vec{q}'\cdot\vec{r}_j)}|0\rangle$$

Assuming that the target nucleus has zero spin, and can be described by LS coupling, one can evaluate the sum

$$M(\vec{q},\vec{q}') = t^{(0)}(\vec{q})\,t^{(0)}(\vec{q}')\,C^{(2)}(\vec{q},\vec{q}') - \frac{3}{N-1}\,t^{(1)}(\vec{q})\,t^{(1)}(\vec{q}')\,\bar{P}^{(2)}(\vec{q},\vec{q}')$$

or using

$$\bar{P}^{(2)}(\vec{q},\vec{q}') = \rho(\vec{q})\rho(\vec{q}') + C^{(2)}(\vec{q},\vec{q}')$$

M becomes

$$M(\vec{q},\vec{q}') = \frac{3}{N-1}\,t_1(\vec{q})\,t_1(\vec{q}')\,\rho(\vec{q})\rho(\vec{q}')$$
$$+ C^{(2)}(\vec{q},\vec{q}')\left[t^{(0)}(\vec{q})\,t^{(0)}(\vec{q}') - \frac{3}{N-1}\,t^{(1)}(\vec{q})\,t^{(1)}(\vec{q}')\right] \tag{2.46}$$

We can now reorder the terms in V_{OPT} so that $V^{(2)}$ involves only correlations, that is the second term in Eq. (2.46). Thus in Eq. (2.34) the terms $t(\vec{q})t(\vec{q}')C(\vec{q},\vec{q}')$ are replaced by $[t^{(0)}(\vec{q})t^{(0)}(\vec{q}') - (3/N-1)t^{(1)}(\vec{q})t^{(1)}(\vec{q}')]$

while Eq. (2.28) becomes:

$$V^{(1)}_{OPT} = (N-1)t^{(0)}(\vec{q})\rho(\vec{q}) + 3(N-1)\int d\vec{k}''\int d\vec{k}'''\, t^{(2)}(\vec{q}')\, t^{(2)}(\vec{q}')\, \rho(\vec{q}')\rho(\vec{q}') \times \langle \vec{k}'' | \frac{1}{\tilde{\alpha}} | \vec{k}''' \rangle \tag{2.47}$$

Because the factor multiplying $\langle \vec{k}'' | \frac{1}{\tilde{\alpha}} | \vec{k}''' \rangle$ factorizes into a function of $\vec{q}$ and of $\vec{q}'$, the Schroedinger equation with this potential can be exactly written as a pair of coupled equations as given in Eq. (2.36) with

$$A = \sqrt{3(N-1)}\; t^{(2)}(\vec{q}')\rho(\vec{q}') \tag{2.48}$$

As one can see from Eq. (2.47) this spin correction is important when

$$\frac{[t^{(2)}(0)]^2}{t^{(0)}(0)} \; \frac{\rho(0)q^3}{k_F^3 E} \gtrsim 1$$

where k_F is the Fermi momentum in units of $\hbar$. The expression on the left is a conservative estimate of the ratio of the second to the first term in Eq. (2.47).

(b) Inelastic Scattering

In this case, the projection operator, P, projects on to the space consisting of the target nucleus in the ground state and in an excited state. The Schroedinger equation now becomes a pair of coupled equations involving these two channels, the elastic and the inelastic. The diagonal components of the coupled channel are identical with $V^{(1)}_{OPT} + V^{(2)}_{OPT}$ of Eq. (2.20). Approximations Eq. (2.28) and Eq. (2.34) apply to the diagonal elastic channel potential. For the inelastic channel potential one need only replace ρ by the ρ for the excited state. The coupling potential between the two channels can be similarly evaluated. Let the excited state be designated by μ, the ground state as before by 0, then the coupling potential $(V_{OPT})_{\mu 0}$ is given by

$$(V_{OPT})_{\mu 0} = (V^{(1)}_{OPT})_{\mu 0} + (V^{(2)}_{OPT})_{\mu 0} \tag{2.49}$$

where

$$(V^{(1)}_{OPT})_{\mu 0} \simeq (N-1)\, t(\vec{q})\, \rho_{\mu 0}(\vec{q}) \tag{2.50}$$

with

$$\rho_{\mu 0}(\vec{q}) = \frac{1}{N}\sum_i \langle \mu | e^{i\vec{q}\cdot\vec{r}_i} | 0 \rangle \tag{2.51}$$

The second order term is given by

$$(V^{(2)}_{OPT})_{\mu 0} = (N-1)^2 \int d\vec{k}'' \int d\vec{k}''' \, t(\vec{k}''-\vec{k}) \langle \vec{k}'' | \frac{1}{\tilde{\alpha}} | \vec{k}''' \rangle t(\vec{k}'-\vec{k}''') \times \left[\bar{\rho}^{(2)}_{\mu 0}\left((\vec{k}''-\vec{k}), (\vec{k}'-\vec{k}''')\right) - \rho_{\mu 0}(\vec{k}''-\vec{k})\rho_{00}(\vec{k}'-\vec{k}''') - \rho_{\mu\mu}(\vec{k}''-\vec{k})\rho_{\mu 0}(\vec{k}'-\vec{k}''') \right] \tag{2.52}$$

The bracket replaces the second order correlation function of the diagonal potential. The quantity $\bar{\rho}^{(2)}_{\mu 0}$ is

$$\bar{\rho}^{(2)}_{\mu 0}\left((\vec{k}''-\vec{k}), (\vec{k}'-\vec{k}''')\right) = \frac{1}{N(N-1)} \sum_{i \neq j} \langle \mu | e^{i\left[(\vec{k}''-\vec{k})\cdot\vec{r}_i + (\vec{k}'-\vec{k}''')\cdot\vec{r}_j\right]} | 0 \rangle$$

These equations have been used by Ullo [2] to discuss inelastic scattering. It is, for example, possible to extend the factorization procedure of section (a') to the coupled equations.

(c) Applications

The Rayleigh-Lax potential, Eq. (2.28), has been used to analyze the scattering of high energy ($\sim$1 GeV) protons by nuclei. Other examples were to be provided by another lecturer. The first two of these is taken from Boridy [7]. Fig. (2.1) compares the elastic scattering calculated using V_{RL} for two differing neutron density distributions, ρ_n. One in which ρ_n does not equal ρ_0, the charge distribution obtained from a Hartree-Fock calculation using a

density dependent Hamiltonian [8]. In the other ρ_n is placed equal to ρ_0. We see substantial differences at the larger angles of scattering. In Fig. (2.2) one can compare the theory using the V_{RL} for elastic scattering and the Tassie model for the inelastic coupling potential rather than the less model dependent result of Eq. (2.50). As one can see, the agreement is excellent indicating that one can in fact determine the neutron density. This is more cogently and clearly seen in Fig. (2.3) in which the difference between the neutron and proton radius is given for the even stable isotopes of Ca [8]. The first three points are obtained from 1 GeV elastic proton scattering. We see that this difference is determined to about ±0.03 fm.

The effects of short range correlation do not make their appearance until one gets to larger scattering angles measured experimentally. However, in order to extract $C^{(2)}$ it will be necessary to carefully estimate the errors in the calculation. We note that the smaller angle diffraction pattern is in excellent agreement with the predictions using the densities of the Pb, Ca and Ni nuclei obtained with the density dependent Hartree-Fock method.

III. Pion-Nucleus Scattering [10,11]

In the preceding discussion of high energy hadron-nucleus scattering, none of the intermediate states were presumed to have a particular importance. The validity of the closure approximation rests upon this hypothesis. We turn now to a case in which a particular intermediate state or better in which a few such states are all important. In the present situation, pion scattering by nuclei, this occurs because these intermediate states are collective and are readily excited by the incident projectile. In other words, these collective states form doorway states for the reaction.

Isolated doorway states such as the giant multiple resonances, the isobar analog resonances, nuclear molecular resonances, Gamow-Teller resonances, shape

isomer resonances and so on are familiar. The collective state responsible for the doorway state resonance is roughly described as a proton particle-proton hole state and a proton particle-neutron hole state in the electric dipole and isobar analog resonance respectively. The relatively long lifetime of these states can follow from an approximate symmetry as in the case of the isobar analog resonance or from dynamical considerations as in the case of the shape isomers (the large potential barrier which inhibits shape changes). Of course, one should remember that the doorway states are not exact eigenfunctions of the nuclear Hamiltonian. Under examination with sufficiently good resolution they fragment into a fine structure. This has been observed in each of the examples cited above.

In the example to be discussed in these lectures, the collective state of the nuclear system is a Δ particle-nucleon hole state. This collective state is formed when a pion strikes a nucleon in the nucleus, the pion being absorbed by it to form a Δ (an excited state of the nucleon with $J = 3/2$ and $T = 3/2$, $E_R = 1232$ MeV, $\Gamma = 115$ MeV) leaving a "hole". As we shall see, a constructively coherent Δ-hole state is formed when the incident pion energy is in the Δ resonance region. Although there is a striking similarity to the particle-hole states mentioned in the preceding paragraph, there is also a most significant difference. In the present case, the particle, the Δ, is unstable. Thus, in this process, it becomes possible for the first time to directly consider the impact of a strongly interacting nuclear environment on a particle resonance. The methods, which are developed for the Δ case, can generally be employed in considering the behavior of other particle resonances such as the Y* inside nuclei.

For the most part many of the theoretical approaches to pion-nucleus scattering have not examined and exploited the possibility of the formation of collective states by the incident pion but have proceeded using some variant

of the multiple scattering theory described in Section II. It was first pointed out by Kisslinger and Wang [12] that the isobar-hole state is a doorway state and could be especially important for elastic and inelastic pion scattering and more generally in reactions in which Δ formation has an important role. The fact that the states formed are collective is the discovery of Hirata, Koch, Lenz and Moniz [10]. It is their work, as well as the results of Lenz, Horikawa and Thies [11] upon which I shall report in this section.

As a first step we shall develop an expression for the resonant pion-nucleon scattering, a representation which will be useful for the later discussion of the pion-nucleus scattering. The projection operator method will be used [13,14]. The equation we wish to solve is the Schroedinger equation

$$H\Psi = E\Psi \tag{3.1}$$

Let the operator P be a projection operator which selects at least the incident channel as well as other states of the system excluding that one which will give rise to the resonance as we shall see. Let the projection operator which selects at least that state be Q so that

$$P + Q = 1 \quad , \quad P^2 = P, \; Q^2 = Q \; , \; PQ = 0 \tag{3.2}$$

Eq. (3.1) then becomes a pair of coupled equations for $P\Psi$ and $Q\Psi$

$$(E - H_{PP})(P\Psi) = H_{PQ}(Q\Psi) \tag{3.3a}$$

$$(E - H_{QQ})(Q\Psi) = H_{QP}(P\Psi) \tag{3.3b}$$

where

$$H_{PP} \equiv PHP, \quad H_{PQ} \equiv PHQ \quad \text{etc.}$$

From Eq. (3.3a) it follows that the $\mathcal{J}$ matrix is

$$\mathcal{J}_{fi} = \mathcal{J}_{fi}^{(P)} + \langle \phi_f^{(-)} | H_{PQ} Q \Psi_i^{(+)} \rangle \tag{3.4}$$

where $\phi_f^{(-)}$ satisfies the homogeneous equation

$$(E - H_{PP})\, \phi_f^{(-)} = 0 \tag{3.5}$$

with the indicated boundary condition. $\mathcal{J}_{fi}^{(P)}$ is the scattering (or reaction) amplitude generated by H_{PP}. The prompt non-resonant processes will be contained in this term. The wave function $\Psi_i^{(+)}$ is the solution of Eq. (3.1) with the appropriate incident wave indicated by the subscript and outgoing wave boundary condition indicated by the superscript.

To determine $Q\Psi_i^{(+)}$ we return to Eq. (3.3) "solving" Eq. (3.3a) as follows:

$$P\Psi = \phi_i^{(+)} + \frac{1}{E^{(+)} - H_{PP}} H_{PQ}(Q\Psi)$$

where $\phi_i^{(+)}$ is also a solution of Eq. (3.5). Inserting this result into Eq. (3.3b) yields

$$\left(E - H_{QQ} - H_{QP} \frac{1}{E^{(+)} - H_{PP}} H_{PQ}\right)(Q\Psi) = H_{QP}\phi_i^{(+)}$$

Inverting, making use of the fact that Q contains no open channels, and inserting the result into Eq. (3.4) yields:

$$\mathcal{J}_{fi} = \mathcal{J}_{fi}^{(P)} + \left\langle \phi_f^{(-)} \middle| H_{PQ} \frac{1}{E - H_{QQ} - H_{QP} \frac{1}{E^{(+)} - H_{PP}} H_{PQ}} H_{QP} \phi_i^{(+)} \right\rangle \tag{3.6}$$

This expression is completely general. Let us now specialize to pion-nucleon scattering. Then the incident system will be designated by the subscript, πn. The interaction H_{PQ} will connect the $\pi + n$ system with the Δ (and other resonances). In the notation of HKLM,

$$H_{PQ} \equiv g_{\pi n \Delta} \quad , \quad H_{QP} = g^{\dagger}_{\pi n \Delta} \tag{3.7}$$

and

$$\Sigma \equiv H_{QP} \frac{1}{E^{(+)} - H_{PP}} H_{PQ} \tag{3.8}$$

The first term $J_{fi}^{(P)}$ just gives the non-resonant scattering. Assuming that only one resonant state, the Δ, is important and that its wave function ψ_Δ is a solution of

$$(\mathcal{E}_\Delta - H_{QQ} - \Sigma)\psi_\Delta = 0$$

Eq. (3.6) becomes

$$J_{fi} = J_{fi}^{(P)} + \frac{\langle \phi_{f,\pi N}^{(-)} | g_{\pi N\Delta} \psi_\Delta \rangle \langle \psi_\Delta | g^{+}_{\pi N\Delta} \phi_{i,\pi N}^{(+)} \rangle}{E - \mathcal{E}_\Delta - \langle \psi_\Delta | \Sigma \psi_\Delta \rangle} \tag{3.9}$$

Note that the "self energy" operator Σ is complex and therefore, in the denominator of the second term, $\langle \psi_\Delta | \Sigma | \psi_\Delta \rangle$ will shift the resonance energy and will also add an imaginary term proportional to the width of the resonance. However, note that since Σ is energy dependent, this width will have an energy dependence. This is of some importance because of the substantial width of the resonance and results in some distortion from the Breit-Wigner form. Eq. (3.9) needs to be revised because of the requirements of special relativity. We shall return to this point in the course of the development which follows.

We turn next to pion-nucleus scattering in the isobar-hole doorway approximation. We employ the methods of my paper with Kerman and Lemmer [14]. First we separate out the doorway state component by further partitioning Q space:

$$Q = \mathcal{D} + q \tag{3.10}$$

where D is the projection operator for the doorway state space. Secondly, the strong doorway state assumption is made; namely that

$$H_{Pq} = 0 = H_{qP} \tag{3.11}$$

but H_{PD} and H_{Dq} and their adjoints do not vanish. This assumption states that the Hamiltonian connects the open channel subspace projected by P only with

the doorway states as is illustrated by Fig. 3.1.

For pion-nucleus scattering, the J matrix given by Eq. (3.6) becomes, after inserting assumption Eq. (3.11),

$$J_{\pi N} = J_{\pi N}^{(P)} + \langle \psi_{f,\pi N}^{(-)} | H_{PD} D \frac{1}{E - H_{QQ} - W_{QQ}^{\uparrow}} D H_{DP} \psi_{i,\pi N}^{(+)} \rangle \tag{3.12}$$

where

$$W_{QQ}^{\uparrow} = H_{QP} \frac{1}{E^{(+)} - H_{PP}} H_{PQ} = H_{DP} \frac{1}{E^{(+)} - H_{PP}} H_{PD} \equiv W_{DD}^{\uparrow} \tag{3.13}$$

We now must calculate $D[1/(E-\tilde{H}_{QQ})]D$ where $\tilde{H}_{QQ} = H_{QQ} + W_{QQ}^{\uparrow}$. To this end let

$$G_{QQ} \equiv \frac{Q}{E - \tilde{H}_{QQ}} \tag{3.14}$$

or

$$(E - \tilde{H}_{QQ}) G_{QQ} = Q$$

Multiplying from the right by D yields

$$(E - \tilde{H}_{QQ}) G_{QD} = \mathcal{D} \tag{3.15}$$

Multiplying from the left by D yields the equation

$$(E - \tilde{H}_{DD}) G_{DD} = \tilde{H}_{Dq} G_{qD} + \mathcal{D} \tag{3.16}$$

while multiplying Eq. (3.15) from the left by q yields

$$(E - \tilde{H}_{qq}) G_{qD} = \tilde{H}_{qD} G_{DD}$$

Inverting this equation and substituting in Eq. (3.16) yields

$$G_{DD} = \frac{\mathcal{D}}{E - H_{DD} - W_{DD}^{\uparrow} - W_{DD}^{\downarrow}} \tag{3.17}$$

where

$$W_{DD}^{\downarrow} \equiv H_{Dq} \frac{1}{E - H_{qq}} H_{qD} \tag{3.18}$$

Hence

$$J_{\pi N} = J_{\pi N}^{(P)} + \left\langle \psi_{f,\pi N}^{(-)} \middle| H_{PD} \frac{1}{E - H_{DD} - W_{DD}^{\uparrow} - W_{DD}^{\downarrow}} H_{DP} \psi_{i,\pi N}^{(+)} \right\rangle \tag{3.19}$$

This is the fundamental formula with which we shall work. The imaginary parts of quantities $W_{DD}^{\uparrow}$ and $W_{DD}^{\downarrow}$ are proportional to the escape and spreading widths respectively.

It is now necessary to fill in this expression taking the Pauli-blocking effect and introducing the necessary modifications required by relativity.

Let us start with H_{PD}. In the isobar doorway model this is given by g, the vertex function described above which converts a nucleon in the target nucleus by the absorption of a pion. This interaction is summed over all the target nucleons taking due account of isospin. The matrix element of g is

$$F_{\Delta N}(\vec{q}) = \langle \Phi(\Delta, 2 \ldots A) | g \Phi_0(1, 2 \ldots A) \rangle \tag{3.20}$$

where Φ_0 is the ground state of the target and Φ is the state produced by pion absorption where $\vec{q}$ is the pion momentum. In an independent particle model

$$F_{\Delta N}(\vec{q}) = \int \frac{d\vec{k}}{(2\pi)^3} \psi_{\Delta}^{*}(\vec{k}+\vec{q})\, \tilde{g}(\vec{\varkappa})\, \psi_m(\vec{k}) \tag{3.21}$$

where ψ_m is the initial nucleon wave function with momentum $\vec{k}$, ψ_Δ is the Δ wave function with momentum $(\vec{k} + \vec{q})$ in units of $\hbar$. The momentum $\vec{\varkappa}$ is the momentum of the pion relative to the center of mass of the nucleon plus pion system:

$$\vec{\varkappa} \simeq \vec{q} - \frac{\omega_\pi}{M_m + \omega_\pi} (\vec{k} + \vec{q}) \tag{3.22}$$

where ω_π is the pion energy/c^2. The quantity $\tilde{g}$ is

$$\tilde{g}(\vec{\varkappa}) = \tilde{f}^{*}\, h(\varkappa^2)\, \vec{\varkappa} \cdot \vec{S}^{+} \tag{3.23}$$

where f^* is the coupling constant modified by some kinematic factors, h is the vertex form factor parametrized as follows

$$\frac{f_{\pi N\Delta}}{m_\pi} h(\varkappa^2) = \frac{A}{1 + \varkappa^2/\alpha^2} \qquad \text{with } A = 25.5 \text{ and } \alpha = 1.8 \text{ fm}^{-1}$$

$\vec{S}$ is a vector operator connecting the spin $\frac{1}{2}$ and spin $\frac{3}{2}$ systems as follows:

$$\langle \tfrac{3}{2} m_\Delta | \vec{S}^{+} | \tfrac{1}{2} m_m \rangle = \sum_m \langle 1 m, \tfrac{1}{2} m_m | \tfrac{3}{2} m_\Delta \rangle \vec{\epsilon}_m$$

where

$$\epsilon_{\pm 1} = \mp (\hat{x} + i\hat{y})/\sqrt{2} \quad , \quad \epsilon_0 = \hat{z}$$

where $\hat{x}$, $\hat{y}$, $\hat{z}$ are unit vectors in the indicated directions.

A second problem is connected with the propagator $(E - H_{DD} \ldots)^{-1}$ in Eq. (3.19) which needs to be given an appropriate relativistic form. This could have been accomplished at the beginning of our analysis by replacing the Schroedinger expression (E - H) by the quadratic Klein-Gordon operator and subsequently employing the projection operator analysis. The energy denominator in the transition amplitude for the pion-free nucleon resonance is then not that given in Eq. (13.9) but is rather D^{-1} where

$$\mathcal{D} = s - m_\Delta^2 + \int dq\, q^2 f(q, k_\Delta) \frac{q^2 h(q)}{q^2 - k_\Delta^2 - i\epsilon} \tag{3.24}$$

where s is the square of the total energy and $(s - m_\Delta^2)^{-1}$ is the "bare" operator while the integral is the "self energy" correction, with the imaginary part proportional to the width.

In the expression for pion nuclear scattering we replace $(E - H_{DD})$ by $D(E - H_\Delta)$ where H_Δ is the Hamiltonian for the Δ-nuclear system

$$H_\Delta = T_\Delta + V_\Delta + H_{A-1}$$

with T_Δ the kinetic energy and V_Δ the potential energy of the Δ inside the

nucleus, while H_{A-1} is the Hamiltonian for the rest of the nuclear system consisting of A-1 nucleons. HKLM use a shell model potential for V_Δ.

In application, $D(E - H_\Delta)$ is linearized:

$$\mathcal{D}(E-H_\Delta) = \mathcal{D}(E) - N_0\gamma(E)H_\Delta \simeq N_0\left(E - E_\Delta + \frac{i\Gamma}{2} - \gamma(E)H_\Delta\right) \tag{3.25}$$

where

$$\partial D/\partial E = N_0\,\gamma(E)$$

Next, consider $W^{\uparrow}_{DD}$, Eq. (3.13). We again replace the propagator by its Klein-Gordon form and therefore write

$$\langle \Delta', (n')^{-1} | W^{\uparrow} | \Delta, n^{-1}\rangle = \int \frac{d\vec{k}}{(2\pi)^3} \frac{F^*_{\Delta' n'}(\vec{k})\, F_{\Delta n}(\vec{k})}{\left(E - \frac{k^2}{2\Delta M_n}\right)^2 - \omega_k^2 + i\varepsilon} \tag{3.26}$$

where F is given by Eq. (3.21).

To evaluate the spreading width $W^{\uparrow}_{DD}$, we adopt the optical model strategy of replacing it by an energy average and then using a phenomenological potential. Upon the assumption that the major source of the spreading width is the absorption reaction

$$\Delta + n \longrightarrow n + n$$

HKLM parametrise $W^{\uparrow}_{DD}$ by $W = V_0\rho(r)/\rho_0$ where ρ is the matter density and V_0 is a parameter. As we shall see Horikawa, Theis, and Lenz found it important to include a spin-orbit term. They use

$$W = W_0\rho(r) + 2\vec{L}_\Delta\cdot\vec{\Sigma}_\Delta\, V^{(0)}_{LS}\,\mu r^2 e^{-\mu r^2} \tag{3.27}$$

where μ and $V^{(0)}_{LS}$ are empirical parameters. For future convenience, we write Eq. (3.27) as follows:

$$W = V_c + 2\vec{L}_\Delta\cdot\vec{\Sigma}_\Delta\, V_{LS}$$

Finally, an ad hoc term is added to take the Pauli-blocking effect into account. Pauli-blocking refers to the forbidden decay of the isobar by pion emission in which the nucleon ends up in an occupied single particle orbit. The free width in D(E), Eq. (3.27), must be corrected for this effect. The correction in the independent particle model is given by

$$\langle \Delta', (n')^{-1} | \delta W | \Delta, n^{-1}\rangle = -\delta_{nn'} \sum_{m,\,occ} \int \frac{d\vec{k}}{(2\pi)^3} \frac{F^*_{\Delta' m}(\vec{k})\, F_{\Delta m}(\vec{k})}{\left[E - (\epsilon_\Delta - \epsilon_m) - \frac{k^2}{2\Delta M_m}\right]^2 - \omega_k^2 + i\varepsilon} \tag{3.28}$$

where ϵ and ϵ are the hole energies.

With the introduction of δW, Eq. (3.19) becomes

$$J_{\pi N} = J^{(P)}_{\pi N} + \langle \psi^{(-)}_{f,\pi N} | g_{\pi m,\Delta} \frac{1}{\mathcal{D}(E) - \gamma(E)H_\Delta - W^{\downarrow}_{DD} - W^{\uparrow}_{DD} - \delta W_{DD}} g_{\Delta,\pi m} \psi^{(+)}_{i,\pi N}\rangle \tag{3.29}$$

where the matrix elements of all the operators which occur have been defined above.

The doorway states are introduced as the eigenstates of the denominator of the propagator:

$$\mathcal{D}(E) - \gamma(E)H_\Delta - W^{\downarrow}_{DD} - W^{\uparrow}_{DD} - \delta W_{DD} | D_i\rangle = (E - E_\Delta + i\Gamma/2 - \epsilon_i) | D_i\rangle \tag{3.30}$$

so that

$$J_{\pi N} = J^{(P)}_{\pi N} + \sum_i \frac{\langle \psi^{(-)}_{f,\pi n} | g_{\pi m,\Delta} | D_i\rangle \langle \vec{D}_i | g_{\Delta,\pi m} | \psi^{(+)}_{i,\pi m}\rangle}{E - E_\Delta + \frac{i\Gamma}{2} - \epsilon_i} \tag{3.31}$$

The calculation of $J_{\pi N}$ thus requires the determination of the solutions of Eq. (3.30) for the doorway states and then substitution in Eq. (3.31). The operator in Eq. (3.30) contains V_Δ which is taken to be proportional to the nucleon density by HKLM with a depth of 55 MeV. The only parameter (complex!) which remains, omitting the spin orbit term in Eq. (3.27) is W_0.

The numerical results revealed a remarkable feature; for example, in the calculation of the transition amplitude for the scattering of 140 MeV pions by ^{16}O for the 0^- partial wave. Harmonic oscillator wave functions were used.

The Δ-hole space was 17 dimensional. The contribution of each of the doorway state solutions is presented in Table 3.1. One immediately sees that one *state D_1 provides by far the largest contribution to the transition matrix.* Moreover, the matrix element of the interaction with the incident channel defined by

$$\frac{|\langle \tilde{D}_1 | g_{\Delta,\pi} \; \psi^{(+)}_{i,\pi N}\rangle|^2}{\langle \psi^{(+)}_{i,\pi N} | g^{\dagger}_{\Delta,\pi m} \; g_{\Delta,\pi m} \; \psi^{(+)}_{i,\pi N}\rangle} \tag{3.32}$$

turns out to be 0.9. D_1 is thus a collective state similar to those seen in the giant multipole resonances.

The fact that the overlap as given by Eq. (3.32) is so large suggests that it would be more economical to use a complete set based upon

$$d_0 \equiv g_{\Delta,\pi m} \, | \psi^{(+)}_{i,\pi N} \rangle \tag{3.33}$$

rather than upon harmonic oscillator wave functions. There is a standard procedure developed by Lanczos (see Morse and Feshbach [15], p. 1155) for developing such a complete set.

Let $\mathcal{H} = \gamma(E) H_\Delta + W^{\downarrow}_{dd} + W^{\uparrow}_{dd} + \delta W_{DD}$

Form the state d_1 from d_0 as follows:

$$d_1 = \mathcal{H} d_0 - \frac{\langle \tilde{d}_0 | \mathcal{H} | d_0 \rangle}{\langle \tilde{d}_0 | d_0 \rangle} d_0 \tag{3.34}$$

Note the orthogonality:

$$\langle \tilde{d}_0 | d_1 \rangle = 0 \tag{3.35}$$

State d_2 is formed by operating on d_1 and orthogonalizing with respect to d_1 and d_0:

$$d_2 = \mathcal{H} d_1 - \frac{\langle \tilde{d}_1 | \mathcal{H} | d_1 \rangle}{\langle \tilde{d}_1 | d_1 \rangle} d_1 - \frac{\langle \tilde{d}_0 | \mathcal{H} | d_1 \rangle}{\langle \tilde{d}_0 | d_0 \rangle} d_0 \tag{3.36}$$

More generally

$$d_\alpha = \mathcal{H} d_{\alpha-1} - \frac{\langle \tilde{d}_{\alpha-1} | \mathcal{H} | d_{\alpha-1} \rangle}{\langle \tilde{d}_{\alpha-1} | d_{\alpha-1} \rangle} d_{\alpha-1} - \frac{\langle \tilde{d}_{\alpha-2} | \mathcal{H} | d_{\alpha-1} \rangle}{\langle \tilde{d}_{\alpha-2} | d_{\alpha-2} \rangle} d_{\alpha-2} \tag{3.37}$$

Not only is d_α explicitly orthogonal to $d_{\alpha-1}$ and $d_{\alpha-2}$, but it is orthogonal to $d_{\alpha-m}$ for $m \leq \alpha$ as well. The proof is left as an exercise. It also follows from Eq. (3.37) that the chaining condition is satisfied by the set d_α:

$$\langle \tilde{d}_\beta | \mathcal{H} | d_\alpha \rangle = 0 \quad \text{unless } \beta = \alpha, \text{ or } \alpha \pm 1 \tag{3.38}$$

From Eq. (3.29) we see that for elastic scattering for a given partial wave one can write

$$J_{n e \Delta} = \langle \tilde{d}_0 | G | d_0 \rangle \Big/ \langle \tilde{d}_0 | d_0 \rangle \tag{3.39}$$

where

$$G = \frac{1}{\mathcal{D} - \mathcal{H}} \tag{3.40}$$

and

$$\mathcal{D} = D(E)$$

Our problem is thus reduced to a calculation of G, or more specifically to expressing G in terms of the set d_α. Define the matrix element of G to be

$$G_{\alpha\rho} = \langle \tilde{d}_\alpha | G | d_\rho \rangle \tag{3.41}$$

In terms of this definition Eq. (3.40) can be rewritten

$$\mathcal{D} G_{\alpha\rho} - \sum_\beta \langle \tilde{d}_\alpha | \mathcal{H} | d_\beta \rangle G_{\beta\rho} = \delta_{\alpha 0}$$

Using the chaining condition, Eq. (3.38), this equation becomes

$$(\mathcal{D} - \mathcal{H}_{\alpha\alpha}) G_{\alpha\rho} = \mathcal{H}_{\alpha,\alpha-1} G_{\alpha-1,0} + \mathcal{H}_{\alpha,\alpha+1} G_{\alpha+1,0} + \delta_{\alpha 0} \tag{3.42}$$

where

$$\mathcal{H}_{\alpha,\beta} \equiv \langle \tilde{d}_\alpha | \mathcal{H} | d_\beta \rangle$$

Let $\bar{\alpha}$ be the value of α for which $\mathcal{G}_{\bar{\alpha}+1,0} = 0$. Eventually we shall let $\bar{\alpha} \to \infty$. Then Eq. (3.42) becomes

$$(\mathcal{D} - \mathcal{H}_{\bar{\alpha}\bar{\alpha}})\, \mathcal{G}_{\bar{\alpha}0} = \mathcal{H}_{\bar{\alpha},\bar{\alpha}-1}\, \mathcal{G}_{\bar{\alpha}-1,0}$$

or

$$\mathcal{G}_{\bar{\alpha}0} = \frac{1}{\mathcal{D} - \mathcal{H}_{\bar{\alpha}\bar{\alpha}}}\, \mathcal{H}_{\bar{\alpha},\bar{\alpha}-1}\, \mathcal{G}_{\bar{\alpha}-1,0}$$

Substituting this result in the equation for $\mathcal{G}_{\bar{\alpha}-1,0}$ yields

$$\left(\mathcal{D} - \mathcal{H}_{\bar{\alpha}-1,\bar{\alpha}-1} - \mathcal{H}_{\bar{\alpha}-1,\bar{\alpha}} \frac{1}{\mathcal{D} - \mathcal{H}_{\bar{\alpha}\bar{\alpha}}} \mathcal{H}_{\bar{\alpha},\bar{\alpha}-1}\right) \mathcal{G}_{\bar{\alpha}-1,0} = \mathcal{H}_{\bar{\alpha}-1,\bar{\alpha}-2}\, \mathcal{G}_{\bar{\alpha}-2,0}$$

Therefore

$$\mathcal{G}_{\bar{\alpha}-1} = \frac{1}{\mathcal{D} - \mathcal{H}_{\bar{\alpha}-1,\bar{\alpha}-1} - \mathcal{H}_{\bar{\alpha}-1,\bar{\alpha}} \frac{1}{\mathcal{D} - \mathcal{H}_{\bar{\alpha}\bar{\alpha}}} \mathcal{H}_{\bar{\alpha},\bar{\alpha}-1}}\, \mathcal{H}_{\bar{\alpha}-1,\bar{\alpha}-2}\, \mathcal{G}_{\bar{\alpha}-2,0}$$

Repeating this process successively and thus reducing the index of $\mathcal{G}$ by one unit each step one eventually arrives at the final expression in the form of a continued fraction for $\mathcal{G}_{00}$

$$\mathcal{G}_{00} = \cfrac{1}{\mathcal{D} - \mathcal{H}_{00} - \cfrac{\mathcal{H}_{01}\mathcal{H}_{10}}{\mathcal{D} - \mathcal{H}_{11} - \cfrac{\mathcal{H}_{12}\mathcal{H}_{21}}{\mathcal{D} - \mathcal{H}_{22} - \cfrac{\mathcal{H}_{23}\mathcal{H}_{32}}{\mathcal{D} - \mathcal{H}_{33} \cdots}}}} \qquad (3.43)$$

The zeros of the denominator in Eq. (3.43) will yield the eigenvalues ε_i of Eq. (3.30).

The efficacy of this procedure is illustrated by Table 3.2, in which the results obtained with N iterations are compared with diagonalization using the harmonic oscillator space. The pion is positive with an energy of 163 MeV and the target nucleus is ^{16}O. It is clear that the process is rapidly convergent, and that even the first term, N = 1, gives excellent agreement with the exact

Table 3.1

i	t_i
1	-.124 + .675i
2	.043 - .066i
3	.034 - .027i
4	.025 - .016i
5	-.005 - .008i
6	.004 - .007i
7	.001 + .003i
8	-.001 - .003i
9	-.004 + .002i
10	.002 - .001i
11	.002 + .001i
12	.000 + .001i
13	.001 + .001i
14	.000 - .001i
15	-.000 + .000i
16	-.000 - .000i
17	.000 - .000i

Table 3.2

	$L^\pi = 0^-$		$L^\pi = 4^-$	
N	Res	ε (MeV)	Res	ε (MeV)
1	.155 + .490i	-53.1 - 154.5i	.060 + .280i	13.9 - 14.4i
2	.159 + .372i	-68.7 - 138.5i	.062 + .246i	-2.7 - 17.7i
3	.154 + .381i	-68.7 - 138.0i	.059 + .251i	-3.4 - 22.7i
"EXACT"	.154 + .381i	-68.7 - 138.0i	.059 + .250i	-3.5 - 23.1i

result. These examples refer to one of the eigenvalues and eigenstates D_i. The number required to obtain the total for the $\mathcal{J}$ matrix for each partial wave is generally very few in number. In this case two states were required for an accurate description of the 4^- transition amplitude and only one for the 0^- partial wave.

The contribution of the various terms is shown in Fig. (3.2) in which the imaginary part of the expectation value of various terms are plotted as a function of pion energy. We see that the dominant term originates in the escape width. The Pauli term does reduce the free space width while the spreading width is of the same order of magnitude as the free space width.

In HLKM, only the first term in the expression for the spreading potential W, Eq. (3.27) is used. The resulting empirical variation for $V_{SP}(0) = \rho(0)W(0)$ is quite severe as can be seen from Fig. (3.3). Horikawa, Theis and Lenz include the spin orbit term as well. The results are shown in Fig. (3.4). As we see, the Re W_0 and the Im W_0 are now roughly independent of pion energy, a much more satisfactory result. Table 3.3 gives the strength $V_{LS}^{(0)}$ and range parameters μ for the spin orbit term.

In Fig. (3.5) and Fig. (3.6) the volume integral of the central term in and the surface integral are given for differing values of the mass number A and compared with values obtained for the nucleon-nucleus interaction:

$$\Omega = 4\pi/(A-1) \int_0^\infty dr\, r^2 (V_0 + \gamma V_\Delta) \quad , \quad S = \int_0^\infty dr\, r\, V_{LS}(r)$$

The comparison of the results of this analysis as carried out by HTL with experiment is shown in the following figures (Fig. (3.7) - (3.13)). Fig. (3.7) compares the computed and experimental absorption cross-section. Fig. (3.8), (3.9) and (3.10) compare the calculated angular distribution with experiment for pion energies of 120, 148, 162, 226, and 260 MeV. The agreement

is good except for the back angles particularly for the 162 MeV case. Figures (3.11), (3.12) and (3.13) compare the scattering from ^{16}O, ^{4}He, and ^{12}C at the indicated energies. From these one can see the very large improvement which results because of the inclusion of a spin-orbit term in Eq. (3.27). The solid line is the result of calculations with, the broken one without, spin-orbit terms. We see the important effects at or near the minima in the angular distributions, filling in or a deepening under different circumstances.

Some discrepancies therefore remain, and one would eventually require a microscopic calculation of the Δ-nucleus interaction as contained in $\mathcal{H}$, rather than the present semi-empirical treatment. Nevertheless it seems fair to say that the elastic pion-nuclear amplitude is well understood, and that one knows how to calculate the behavior of the Δ-resonance inside the nucleus. Obviously the theoretical treatment of various processes in which the pion is involved must take advantage of this increased understanding. The doorway states need not decay only into the elastic channel. In other words, inelastic scattering, pion production or absorption, photoproduction and radiative capture may pass through the doorway states revealed by the above discussion of elastic scattering.

Finally, returning to a theme discussed earlier, the same methods developed in this section should also prove useful for other baryon resonances such as the Y* which is produced when a K^- is absorbed by a nucleon. Moreover, it may also be a useful way in which to treat the familiar giant resonances.

IV. Hypernuclei [16]

We turn next to the case where the baryon probe is the relatively stable strange particle, the Λ, or possibly the Σ. This is to be contrasted with the situation discussed in Sec. III, in which the baryon is the much less stable Δ.

Table 3.3

	$\mu(fm^{-2})$	$V_{LS}^{(0)}$(MeV)
π - ^{4}He	0.25	-4.6 - 1.8i
π - ^{12}C	0.35	-10 - 4i
π - ^{16}O	0.3	-10 - 4i

Although Λ hypernuclei were known from experiments involving emulsions for some time, it was not until the use of a nearly recoiless method of production in the pioneering experiments of Bressani et al. [17] and Povh et al. [18] that hypernucleus physics attracted the attention of the nuclear physics community. The recoiless method [19] is based on the observation that in the elementary process

$$K^- + n \longrightarrow \Lambda^0 + \pi^- \tag{4.1}$$

when the pion is observed in the forward direction a kaon momentum exists for which the Λ^0 produced is at rest. This result is illustrated in Table 4.1 and Fig. (4.1). Fig. (4.1) also contains a plot of the cross-section for forward production of pions according to process Eq. (4.1) indicating some advantage in using kaon beams whose momentum is not exactly at the critical 540 MeV/c.

It would be expected that the production of Λ hypernuclei will be enhanced when the kaon momentum is near 540 MeV/c and the pions are observed in the forward direction. The reaction is

$$K^- + {}^{Z}A \rightarrow {}^{Z}_{\Lambda}A + \pi^- \tag{4.2}$$

Because of the small momentum transfer a neutron in the target nucleus is simply replaced by a lambda. By observing the spectrum of the pions one will be able to determine the spectrum of the hypernucleus formed, subject of course to whatever selection rules apply at 0°.

Similarly Σ hypernuclei can be formed. The elementary interactions are

$$K^- + n \longrightarrow \Sigma^0 + \pi^- \qquad \text{(a)}$$

$$K^- + p \longrightarrow \Sigma^+ + \pi^- \qquad \text{(b)} \qquad (4.3)$$

$$K^- + p \longrightarrow \Sigma^- + \pi^+ \qquad \text{(c)}$$

Table 4.1

p	0	400	540	700	1000	2000	MeV/c
p_Λ	250	40	0	40	75	130	MeV/c

Note the possible formation of a π^+ which has an enhanced detection. The incident kaon beam generally contains many negative pions and negative pions are produced by the decay of the K^- in flight.

Examples of the formation of Λ hypernuclei [21] are shown in Fig. (4.2). Relatively sharp states have been observed. The formation of Σ hypernuclei is indicated in Fig. (4.3) [22]. The peak corresponding to the Σ hypernucleus should occur at the same excitation energy whether the process involves the production of a π^- or a π^+. This is certainly the case for at least one of the structures involved. In these experiments p_k = 720 MeV/c while the momentum transfer is 130 MeV/c. Σ states were seen in ^{9}Be and ^{7}Li as well.

I shall not attempt to summarize all the experimental and theoretical issues of interest. Two particular points seem to me to be especially interesting.

(a) The first refers to the question: Why are there Σ hypernuclear states in $^9_\Sigma$Be, $^7_\Sigma$Li, and $^{12}_\Sigma$C which are relatively narrow? The existence of these states is a surprise because of the expected rapid conversion to a Λ hypernucleus via the strong interaction process $\Sigma + n \to \Lambda + n$. An estimate obtained by Batty is confirmed by Gal and Dover [23] for the case of nuclear matter. In that case the width is given by

$$\Gamma \sim \overline{v\sigma_c} \langle \psi | \Sigma\, \delta(\vec{r}_\Sigma - \vec{r}_i) | \psi \rangle \qquad (4.4)$$

where v is the velocity of the Σ - p pair converting with total cross-section, σ_c. The bar represents the average over the Fermi gas used to describe the Λ hypernucleus. The wave function ψ is that of the Σ hypernucleus. The results are given in Table 4.2.

According to Gal and Dover, the reduction in the conversion rate from that calculated using Eq. (4.4) is a consequence of the fact that the elementary process, $\Sigma + n \to \Lambda + n$, is dominated by the $T = \frac{1}{2}$, $S = 1$ channel (Engelmann [24]). One should therefore replace $\langle \psi | \Sigma_i \delta(\vec{r}_\Sigma - \vec{r}_i) | \psi \rangle$ by

Table 4.2

Γ_1^Σ = 22 MeV

nucleus	^{7}Li	^{9}Be	^{12}C	^{16}O	
Γ_{1p}^Σ	6.8	8.8	15.0	14.7	MeV

$$\langle\Psi|\sum_i \delta(\vec{r}_\Sigma-\vec{r}_i)\left(\tfrac{1}{3}-\tfrac{1}{3}\vec{t}_\Sigma\cdot\vec{\tau}_i\right)\left(\tfrac{3}{4}+\tfrac{1}{4}\vec{\sigma}_\Sigma\cdot\vec{\sigma}_i\right)|\Psi\rangle \tag{4.5}$$

where the spin and isospin factors project upon the triplet spin and $T = \frac{1}{2}$ isospin for the (Σ,n) pair. Note that $\vec{t}_\Sigma$ is chosen so that $t_\Sigma^2 = 2$.

Under the experimental conditions the states most likely to be excited at 0° for the ^{12}C target are given in Table 4.3. In this table, the nucleon, Σ configuration is given together with the possible isospins of the final Σ hypernucleus. The quenching factor, Q, that is the factor multiplying the values obtained using Eq. (4.4) given in Table 4.2 which is generated if that expression is replaced by Eq. (4.5) is given in Table 4.4. From this analysis one would expect that only the T = 3/2 0^+ state should be visible with a width given by 0.4 × 14.7 ∿ 6 MeV. Presumably this is the state seen in Fig. (4.3).

Dover and Gal have carried out similar calculations for ^7Li and ^9Be. These are summarized in Table 4.5, where T_N refers to the isospin of the core nucleus to which the Σ is bound. The two lines in the ^9Be case correspond to the assumption that the spin of the core nucleus is zero for the upper line and one for the lower line. In ^7Li one would expect the T = 2 state to be observable while for ^9Be, the levels seem to be $S_N = 1$, $T_N = 1$ and T = 2 for the upper peak and $S_N = 0$, $T_N = 0$, and T = 1 for the lower peak.

Predictions for an ^{16}O target are given in Table 4.6. At least one state should be observable. If the Σ spin orbit force is weak, two would be expected. Clearly it is of great interest to understand the mechanism responsible for the narrow Σ hypernuclear states and in particular to see if the correct one is that suggested by Dover and Gal. That understanding will reflect itself in a greater insight into the nature of the transition $\Sigma + n \rightarrow \Lambda + n$.

Table 4.3

J^Π	$0^+(p_{3/2}^{-1}, p_{3/2})$	$1^-(p_{3/2}^{-1}, 1/2)$
$^{12}C(K^-,\pi^-)$	T = 1/2, 3/2	T = 1/2, 3/2
$C(K^-,\pi^+)$	T = 3/2	T = 3/2

Table 4.4

J^{Π}	0^+		1^-	
	T = 1/2	3/2	T = 1/2	3/2
Q	1.42	0.41	1.17	0.86

Table 4.5

	^{7}Li				^{9}Be				
					lower peak	upper peak			
(T_N,T)	(0,1)	(1,0)	(1,1)	(1,2)	(0,1)	(0,1)	(1,0)	(1,1)	(1,2)
Q	0.92	2.65	2.00	0.71	0.78	1.22	1.93	1.64	1.02
							2.01	1.29	.70

Table 4.6

	$0^+(p^{-1}_{3/2}, p_{3/2})$		$(p^{-1}_{1/2}, p_{1/2})$		with strong Σ spin orbit coupling $^1S_0$		$^3P_0$	
T	1/2	3/2			1/2	3/2	1/2	3/2
Q	1.32	0.56	1.19	0.81	1.44	0.30	1.06	1.06

(b) In this second section on hypernuclear physics, I wish to pay especial attention to the role of the Λ in the hypernucleus as a probe of nuclear structure [25]. The conditions under which the Λ does act as a probe can be formulated as follows. A 0'th order approximation for the hypernuclear wave function is

$$\Psi^{(0)}_{\alpha a} = \chi^{(\Lambda)}_{\alpha} \; \psi^{(core)}_{\alpha} \tag{4.6}$$

where $\chi^{(\Lambda)}_{\alpha}$ is the single particle state of the Λ, ψ_a is the wave function for the nuclear core in the state a. Consider the first order correction to this zeroth order wave function as given by first order perturbation theory. This correction will involve excitations of the state of the Λ and that of the core. Since the single particle levels are separated by much greater values of the energy than the core excitations, the latter will dominate unless of course some special conditions reduce the value of the excitation matrix element. Assuming this does not occur the expression for $\Psi_{\alpha a}$ good to the first order has the form:

$$\Psi_{\alpha a} = \chi^{(\Lambda)}_{\alpha} \left\{ \psi^{(core)}_{a} + \sum_{a \neq b} \frac{\langle \psi^{(core)}_{a} | V_{\alpha} \psi^{(core)}_{b} \rangle}{E_a - E_b} \psi^{(core)}_{b} + \dots \right\} \tag{4.7}$$

where

$$V_{\alpha} = \langle \chi^{(\Lambda)}_{\alpha} | V_{\Lambda n} | \chi^{(\Lambda)}_{\alpha} \rangle \tag{4.8}$$

The probing potential acting on the nuclear core is, in this approximation, given by the residual Λ-nucleon potential average over the Λ density. As a consequence the energy levels and the electromagnetic transition probabilities will be altered. It is clear that this effect will be most dramatic when $\psi^{(core)}_b$ are low lying collective states. That this description is qualitatively correct is demonstrated by Gal and Dalitz [26] more careful calculation of the levels of $^{12}_{\Lambda}C$ as seen in Fig. (4.4). Moreover, the DWIA calculations

of Dover et al. [27] shown in Fig. (4.5) and Fig. (4.6) give excellent fits to the angular distribution of the reactions $^{12}C(\pi^-,\pi^-)^{12}C^*$. Their magnitudes must however be reduced by the indicated factors. The 1^- state is clearly resolved. In Fig. (4.6) one assumes that the measured excitation is a sum of the excitation of the 0^+ and the two 2^+ states. Note that the contribution of the $_\Lambda p_{3/2}$ and $_\Lambda p_{1/2}$ orbitals are included. The levels associated with the latter are shown in Fig. (4.4). At small angles the angular distribution is dominated by the 0^+ state. The presence of the 2^+ contribution is indicated by the shoulder in the experimental angular distribution. The need for substantial corrections to the magnitude is not surprising in view of the rough character of these calculations.

For heavier nuclei one can expect the Λ to modify the collective parameters such as the radius or the moment of inertia. The modification of the radius is similar to the isotope shift in atoms. The change in the parameter r in the formula $R = r A^{1/3}$ from its Λ free value r_0 is given by

$$r = r_0 \left[1 - \frac{B_\infty + B_\Lambda(A)}{KA} \right] \tag{4.9}$$

where A is the mass number of the core, K is the nuclear compressibility, B_∞ and $B_\Lambda(A)$ are the binding energies for the Λ for A infinite and for A finite. Taking K = 150 MeV, $(r - r_0)/r_0$ for ^{15}N = .026. It is anticipated that this effect would be visible in the Coulomb energies of hypernuclei once the nuclei are sufficiently large so that the charge symmetry breaking force becomes unimportant. The influence of three-body forces has also been neglected in deriving Eq. (4.9).

As a second example of the effect of the Λ I shall discuss the moment of inertia of a hypernucleus using the deformed harmonic oscillator model. The change in the moment of inertia due to the Λ is given by

$$\Delta \mathcal{J} = M_\Lambda R_0^2 \left[\left(\tfrac{4\pi}{3\sqrt{5}} \beta^2 + \dots\right)(n_y + n_z + 1) + \sqrt{\tfrac{4\pi}{5}} \left(\tfrac{2}{3}\beta + \dots\right)(n_z - n_y) \right] \tag{4.10}$$

where as usual R_0 and β are defined by the equations

$$\langle z^2 \rangle^{\frac{1}{2}} = R_0 \left(1 + \sqrt{\tfrac{5}{4\pi}}\beta\right) \qquad \langle x^2 \rangle^{\frac{1}{2}} = R_0 \left(1 - \tfrac{1}{2}\sqrt{\tfrac{5}{4\pi}}\beta\right)$$

so that β measures the deformation. The values of n_y and n_z give the quantum numbers of the Λ orbital. The first term in Eq. (4.10) is the so called irrotational flow term so that there is an opportunity to observe this term directly. One should note that Eq. (4.10) does not give the total change in the moment of inertia since the deformation β will change because of the presence of the Λ.

It should be quite clear from these examples that the Λ will change the properties of the core nucleus. It is not so clear that it will be experimentally possible to observe the spectra of the appropriate hypernuclei. Looking for the γ-decays seems to be the most attractive possibility.

V. The Collision of Ultra-Relativistic Hadron Projectiles With Nuclei [28,29]

The collision of ultra-relativistic hadron projectiles with nuclei appears to involve reaction mechanisms which differ qualitatively from those which govern the three types of reactions we have discussed in Sections II, III and IV. We will be dealing with projectiles whose energies are at least several times the rest energy of the projectile. Not unexpectedly, special relativity plays an important role. But in addition the interaction between the incident hadron and the nucleon in the target nucleus is qualitatively different in nature from the interaction which prevails at a lower energy. The evidence for these remarks is presented in (a).

(a) We present first the rather startling results obtained by studying the collision of high energy protons with nuclei. Generally, the target nuclei are heavy, e.g. U or Au, the particles detected are fragments of the target,

and the means of detection are radiochemical although one of the experiments to be reported employs counter detectors.

The phenomena of interest are illustrated in Figs. (5.1), (5.2) and (5.3) [30,31]. In the first of these the average energy of a recoiling fragment in the laboratory frame of reference formed in the reaction p + U is plotted. We see that beginning at a few GeV as the proton energy increases the average fragment energy decreases. This is the opposite of what happens at lower proton energies where an increase in proton energy is reflected by an increase in fragment energy. The fragment angular distribution as indicated by the forward to backward ratio, F/B, of Fig. (5.2) becomes more peaked in the forward direction as the proton energy increases from 1 GeV till about 5 GeV. For greater proton energies the angular distribution has been obtained at 28 GeV. In Fig. (5.3) we see that the angular distribution of the Fourine fragment is rather flat with a peak at 70° in the laboratory frame. These results imply that collisions of the proton with the nucleons inside the nucleus do not result in energy being transferred to nuclear degrees of freedom. The first surmise is that in fact the internal degrees of freedom being excited are those of the nucleon and that the excited nucleon does not in fact transfer its excitation to other nucleons in the form of kinetic energy.

It is in fact well known that, at least at high energies (>60 GeV), this process of nucleon or more generally hadron excitation is dominant in the kinematic region corresponding to non-peripheral reactions. The evidence is provided by measurement of the multiplicity of high energy ($\beta > 0.7$) charged particle production. These measurements show that the number of such particles rises very slowly with increasing mass number as shown by Fig. (5.4) and Table 5.1 [32]. No cascading is indicated as cascading would result in a much more rapid rise in the multiplicity with increasing mass number. The explanation is again that very little energy is deposited in the nucleus.

Table 5.1

The average multiplicities of relativistic charged particles produced in 100 - GeV/c hadron-nucleon collisions. From Ref. [32].

Target	Projectile	Average Multiplicity
C	π^+	7.86 ± 0.15
	K^+	6.92 ± 0.33
	p	7.72 ± 0.16
Cu	π^+	10.29 ± 0.26
	K^+	8.89 ± 1.10
	p	11.00 ± 0.32
Pb	π^+	13.21 ± 0.30
	K^+	12.92 ± 0.79
	p	14.75 ± 0.38
U	π^+	14.57 ± 0.39
	K^+	12.93 ± 1.33
	p	15.94 ± 0.50
Hydrogen (bubble chamber)	π^+	6.62 ± 0.07
	K^+	6.65 ± 0.31
	p	6.37 ± 0.06

Empirically the multiplicity ratio, R, the ratio of the multiplicity in nuclei to that in hydrogen is given by

$$R = 1 + \frac{1}{2}(\nu - 1) \tag{5.1}$$

where ν is the mean number of collisions.

The explanation is quite interesting. Upon the collision of the incident hadron with a target nucleon, the hadron and the target nucleon are excited. As a consequence the wave function for the excited hadron can be decomposed into a linear combination of states each with its own characteristic lifetime τ_0 for decay into incident hadron plus a number of pions. This lifetime is of course given in the rest frame. In the laboratory frame the lifetime is

$$\tau = \frac{E}{m}\tau_0 \tag{5.2}$$

where E is the total kinetic energy of the state with lifetime τ_0. There can very well be several τ_0's corresponding to the many excitation possibilities. However a rough average energy $\bar{E}$ can be obtained by assuming that this new entity, the excited hadron, is at rest in the center of mass system of the hadron plus nuclear nucleon. Under these circumstances

$$\bar{E}/m = (E_{lab}/2mc^2)^{\frac{1}{2}} \tag{5.3}$$

The corresponding value of τ, $\bar{\tau}$, is

$$\bar{\tau} = (E_{lab}/2mc^2)^{1/2}\tau_0 \tag{5.4}$$

The critical value of $\bar{\tau}$ is given by $c\bar{\tau} \equiv \ell \sim \lambda$ where λ is the mean free path of a hadron inside a nucleus. If ℓ is larger than λ, the excited hadron will not have decayed appreciably before it has its second collision. The second collision reconstitutes the excitation in the hadron and the decay is halted. Under these circumstances, $\ell > \lambda$, the hadron will pass through the

nucleus without decaying, decaying by emission of a number of pions only after it has left the nucleus. The result for R is obtained if one assumes that there is a component generated at each collision, which decays after leaving the nucleus, with an average energy given by E^{α} and the multiplicity by $\log E^{\alpha}$ where $\alpha = 1/2$.

The critical energy at which nucleon excitation should dominate in the production of fast secondaries can be obtained from $\ell \sim \lambda$. Placing $\ell \sim 2$ fm and $\ell \sim 1$ fm, one obtains $E_{lab} \sim 8$ GeV. This is in rough accord with experiment, but of course a more quantitative development of these ideas is required before a critical evaluation is possible and before one can say that the underlying causes of the phenomena noted in Figs. (5.1)-(5.3) and Fig. (5.4) identical.

The momentum transfer to the nucleus by the incident hadron is thought to be relatively small. The transferred transverse momentum, on the basis of experimental data presently available, is relatively independent of the projectile energy. It is thought to be of the order of about 400 MeV/c leading to an energy of 80 MeV per nucleon. The value of the longitudinal momentum transfer is not clear. If it is substantial, the incident hadron would drill a hole through the nucleus. If it is relatively small the nucleons in the nucleus would instead be pushed aside. The model described above, which is based upon Gottfried's analysis, presumes a relatively small longitudinal momentum transfer, the generation of the observed relativistic multiparticle states being associated with the leading incident particle. However other models which have been used would predict the formation of a hole in the target nucleus. The question of the magnitude of the transfer of longitudinal momentum needs experimental investigation. Its value is intimately related with the magnitude of the average excitation of the nucleon.

(b) The collision of a relativistic heavy ion with a nucleus may involve a "central" collision characterized by the production of a large number of particles with substantial values of the transverse momentum [27,32]. It may involve a "peripheral" reaction which leads to a fragmentation of the incident projectile. The fragments, in this case, move with the velocity of the incident projectile and in the forward direction in the laboratory reference frame. As a consequence this component of the reaction can be readily selected experimentally. At the present time the fragmentation process is understood at the level of the prevailing experimental uncertainties. There is no corresponding level of understanding of the central collision. The "fire ball" hypothesis first invoked has proven inadequate, being unable to provide an explanation of the experimental data. A substantial improvement has been made by adding an initial blast wave [33], but the theory still involves the unwarranted assumption of thermal equilibrium.

This lecture will restrict itself to the peripheral reactions. Not enough time is available for an adequate description of the central collisions, the fireball and its modifications as well as of the other models which are being developed.

The method to be described below [28,29] is referred to as the "nuclear Weiszäcker-Williams method". First let us summarize the experimental facts obtained by experiments performed at the Bevalac facility [34]. Experiments were performed with a beam of energetic projectiles (e.g. ^{16}O) at energies of 1.05 GeV/A and 2.1 GeV/A. Projectile fragmentation was detected by observing reaction products in the forward direction. Inclusive cross-sections, that is cross-sections for the production of a particular nuclear fragment without a determination of the correlated production of other fragments were measured. The results obtained are most simply expressed with respect to the projectile frame of reference defined as that frame in which the incident projectile is

at rest and the target nuclei effectively form the incident beam.

a. In the projectile frame, the momentum of a fragment is relatively small. For example, if the target nucleus is Pb, its momentum in the projectile frame is (208) × (2.1) ∿ 437 GeV/c when the projectile has an energy of 2.1 GeV/A. The longitudinal momentum, p_L, distribution of ^{10}Be fragments produced by fragmentation of the projectile, ^{12}C, in the projectile frame is shown in Fig. (5.5). We see that the ^{10}Be average longitudinal momentum is only about 50 MeV/c, while the dispersion of the p_L distribution is about 100 MeV/c, which should be compared with the 437,000 MeV/c carried by the Pb nucleus. Thus a very small fraction (10^{-4}) of the momentum of the lead nucleus is transferred to the projectile.

b. The distribution, $w(p_L,\vec{p}_T)$, in the longitudinal, p_L, and transverse components, $\vec{p}_T$, of the momentum is Gaussian in each. Empirically one finds that

$$w(p_L,\vec{p}_T) \sim \exp\left\{-\left[\frac{1}{2\sigma_L^2}(p_L-\bar{p}_L)^2+\frac{1}{2\sigma_T^2}p_T^2\right]\right\} \tag{5.5}$$

where $\bar{p}_L$ as mentioned above is generally several tens of MeV/c.

c. The angular distribution is approximately isotropic, that is

$$\sigma_L \simeq \sigma_T \tag{5.6}$$

However because of the much greater experimental difficulty in the determination of the transverse momenta, Eq. (5.6) must be considered as approximate.

d. The dispersion, σ_L, is empirically independent of A_T (the target mass number) depending only on A_F (the fragment mass number) and A_P (the projectile mass number). This is a first example of independence of the projectile fragmentation of A_T.

e. A second is given by the fact that the branching ratio for the relative probability for the production of a fragment type is independent of the

target nucleus. The cross-section for the production of a fragment F, upon the collision of a target T with a projectile P is found to be

$$\sigma_{PT}^{(F)} = \sigma_{PT} \frac{\gamma_P^{(F)}}{\gamma_P} \quad \text{where} \quad \sum_F \gamma_P^{(F)} = \gamma_P \tag{5.7}$$

The ratio, multiplying σ_{PT}, is the branching ratio for the production of fragment F.

f. The inclusive cross-section σ_{incl} is proportional to the radius of the interaction. Empirically

$$\sigma_{incl} \sim A_P^{\frac{1}{3}} + A_T^{\frac{1}{3}} - 0.8 \tag{5.8}$$

g. Cross-sections and σ_L at 1.05 GeV/A and 2.1 GeV/A are approximately the same indicating within this energy range independence with respect to the energy.

h. *The momentum distribution of the emergent protons is not Gaussian.* It is better described by an exponential, e^{-p/p_0}, where $p_0 \sim 65$ MeV/c.

We shall now discuss the momentum distribution of the fragments.

(a) Momentum Distribution of Projectile Fragments

The model we shall use was first suggested in Ref. [35]. The derivation employed below follows essentially that of A. Goldhaber [36]. The model assumes that the fragment of mass number, A_F, is formed from the projectile of mass A_P by removing the binding of a group of A_F nucleons. The net momentum $\vec{P}_F$ of the fragment is then obtained by adding up the momentum of each of these nucleons. The value of $\vec{P}_F$ will vary according to which group of A_F nucleons is selected from the projectile giving rise to a distribution in $\vec{P}_F$. If the mean square momentum of a nucleon in the projectile is $\langle p^2 \rangle$, the mean square value of $\vec{P}_F$ is, according to a simple statistical considera-

tion,* given by $A_F \langle p^2 \rangle$. The distribution in $\vec{P}_F$, following again from statistical considerations [35], is Gaussian** at least in the neighborhood of the maximum of the distribution. This occurs near $P_F = 0$ since the average momentum of the fragments is so close to zero. Note that this model automatically assumes that the projectile fragment distribution does not depend upon the nature of the target.

Suppose then that the projectile breaks up into fragments of mass number A_i so that

$$\sum A_i = A_P \tag{5.9}$$

Let the momentum of each fragment be $\vec{P}_i$. Assume that the distribution of momenta for the i'th fragment depends only upon $\vec{P}_i$ and is Gaussian. Then the momentum distribution, w, for a given set of A_i is:

$$w(\vec{P}_1, \vec{P}_2 \ldots) \sim \prod_i \exp\left[-\tfrac{2}{3} P_i^2 / A_i \langle p^2 \rangle\right] \tag{5.10}$$

To obtain the observed inclusive momentum distribution we must integrate over all momenta except that of the observed fragment, say A_1, subject to the condition

$$\sum_i \vec{P}_i = 0 \tag{5.11}$$

---

*Assume that $\vec{P}_F = \Sigma \vec{p}_\mu$ where $\vec{p}_\mu$ are the momenta of the nucleons making up the fragment. Then $P_F^2 = \Sigma p_\mu^2 + \sum_{\mu \neq \nu} \vec{p}_\mu \cdot \vec{p}_\nu$. Averaging over the momentum distribution of the projectile nucleons, we find $\langle \sum_{\mu \neq \nu} \vec{p}_\mu \cdot \vec{p}_\nu \rangle = 0$. Hence

$$\langle P_F^2 \rangle = \langle \sum_\mu p_\mu^2 \rangle = A_F \langle p^2 \rangle$$

**This result follows simply from the assumption that the momentum distribution is symmetric about the maximum.

As shown by experiment the average momentum of a projectile fragment in the projectile frame of reference is very small justifying to some extent Eq. (5.11). Hence the single fragment distribution, $w(\vec{P}_1)$, is given by

$$w(\vec{P}_1) = \int w(\vec{P}_1, \vec{P}_2 \ldots)\, \delta(\Sigma \vec{P}_i)\, d\vec{P}_2 \ldots \tag{5.12}$$

This integral may be easily performed to yield

$$w(\vec{P}_1) \sim \exp\left(-P_1^2/2\sigma^2\right) \tag{5.13}$$

where

$$\sigma^2 = \frac{1}{3}\langle p^2\rangle (A_p - A_F) A_F / A_p \tag{5.14}$$

If we adopt the Fermi-Gas model as a description of the projectile nucleus

$$\frac{1}{3}\langle p^2\rangle = \frac{1}{5} p_F^2 \tag{5.15}$$

where p_F is the Fermi momentum.

The experimental results are shown in Fig. (5.6). As can be seen from Fig. (5.6), the dependence of σ^2 on A_p and A_F, given by Eq. (5.14), is verified by experimental data. However that data yields a value for p_F (according to Eq. (5.14)) equal to 190 MeV/c whereas the value of p_F determined from quasi-elastic electron scattering is, for ^{16}O, given by 225 MeV/c. As suggested by Hüfner this discrepancy may occur because fragmentation occurs only after the emission of a number of nucleons. The fragmenting nucleus is not ^{16}O but a lighter nucleus with a correspondingly lower value of p_F.

The distribution given by Eq. (5.10) can also be used to calculate the angular correlation between two fragments, A_1 and A_2, which exists in virtue of Eq. (5.11). One obtains

$$w(\vec{P}_1, \vec{P}_2) \sim \exp\left\{-\frac{2}{3\langle p^2\rangle}\frac{1}{A_p - A_1 - A_2}\left[P_1^2\frac{A_p - A_2}{A_1} + P_2^2\frac{A_p - A_1}{A_2} + 2\vec{P}_1\cdot\vec{P}_2\right]\right\}$$

This implies a greater probability for the two fragments to go off in opposite directions. Determination of this angular correlation would provide a test of the independence hypothesis as formalized by Eq. (5.10). It appears however to be very difficult to carry out this experiment.

(b) *The Nuclear Weiszäcker-Williams Method* [29]

The Weiszäcker-Williams method relates the reaction cross-section induced by a charged particle to that induced by a distribution of photons. The electromagnetic field of a rapidly moving charged particle can be shown to be approximately equivalent to a beam of photons with the frequency distribution

$$n(\omega)\, d\omega = \frac{2}{\pi}(Z\alpha)^2 \frac{d\omega}{\omega} \tag{5.16}$$

where Z is the charge of the particle and α is the fine structure constant. The cross-section for a reaction induced by a charged particle is given then in terms of the cross-section $\sigma_\gamma(\omega)$ for the photon induced reaction by

$$\sigma = \int n(\omega)\, \sigma_\gamma(\omega)\, d\omega = \frac{2}{\pi}(Z\alpha)^2 \int \frac{\sigma_\gamma(\omega)}{\omega}\, d\omega \tag{5.17}$$

In this section a theory of the fragmentation of a relativistic heavy ion projectile will be developed. The expression for the cross-section, which will be obtained, will have a structure similar to that of Eq. (5.17) so that the theory will be referred to as the "Nuclear Weiszäcker-Williams" method.

The projectile reference frame will be used. In that frame it will be assumed that the target nucleus travels without deviation and without internal excitation in a straight line. This assumption is indicated by experimental result (a) which demonstrates that the momentum transferred to the projectile nucleus by the target nucleus is small. It is identical with the assumptions made in developing the electromagnetic Weiszäcker-Williams result. However,

after the target nuclei has penetrated into the projectile a distance, λ, approximately equal to a nucleon mean free path, a strong collision with large momentum transfer will occur. This collision will not contribute to the process being considered since the reaction products will fall outside of the small forward cone where the fragments are detected. This competitive process is taken into account by assuming that the probability of finding the target nucleus intact attenuates during the collision with a scale measured by the mean free path, λ.

It is assumed that the collision is peripheral. This result is implied very directly by experimental result (f) as given in Eq. (5.8). The mean free path, λ, used is the value valid on the surface region of the interacting nuclei.

A qualitative description of the consequences of these assumptions can be given. The projectile nucleons feel a pulse of force as the target nucleus passes by. The duration of the pulse, τ, is given by the scale, λ, Lorentz contracted to λ/γ, divided by the velocity of the projectile, v, which is very close to c, the velocity of light. Thus

$$\tau \sim \lambda/\gamma v \tag{5.18}$$

where

$$\gamma = (1 - v^2/c^2)^{-1/2} = E/m_A$$

where v is the velocity of the target and E is its energy. From the duration of the pulse one can calculate the maximum* energy transfer $\hbar\omega_c$ which can occur:

$$\hbar\omega_c \sim \hbar/\tau = \gamma\hbar v/\lambda \tag{5.19}$$

*By "maximum" we shall mean the value of $\hbar\omega$ at which the cross-section is 1/e of its value for very small values of $\hbar\omega$.

For a target energy of 2.1 GeV/A and λ = 1.75 fm the maximum energy transfer is found from this equation to be 365 MeV. We see immediately that we are in fact dealing with a comparatively low energy phenomenon. There will be other effects to be discussed below which will reduce the maximum energy transfer to even considerably lower values.

Following an argument of Brown and Deutchmann one can estimate the corresponding momentum transfer $\hbar q_{L,c}$. That momentum transfer is given roughly by

$$\hbar q_{L,c} \sim \frac{\gamma\hbar}{\lambda} = \hbar\omega_c/v \tag{5.20}$$

This is thus a relatively small momentum. For the case discussed above, the maximum momentum transfer is thus 365 MeV/c. Recall that the Fermi momentum for a heavy nucleus is about 260 MeV/c while for the ^{16}O nucleus it is 225 MeV/c as mentioned above. Relationship (5.20) is valid more generally as we shall show below; that is the longitudinal moment transfer, $\hbar q_L$, is related to the energy transfer as follows

$$\hbar q_L = \hbar\omega/v \tag{5.21}$$

The maximum value of transverse momentum transfer, $\hbar q_T$, is determined by the transverse scale of the target density, namely a, the parameter measuring the thickness of the nuclear surface. The maximum transverse momentum transfer is thus

$$\hbar q_{T,c} \sim \hbar/a$$

For a ~0.6 fm, $\hbar q_{T,c}$ is about 333 MeV/c.

In addition to these cut-offs in q_T and q_L which come from the shape of the interacting nuclei, additional cut-offs which have a dynamic origin must be taken into account. The most obvious of these is the momentum transfer

which the nucleon-nucleon potential will allow before a substantial reduction in the amplitude will occur. From the empirical expression for the nucleon-nucleon amplitude [37], we find that the nucleon-nucleon potential produces a momentum cut-off, for both the transverse and longitudinal components, of 370 MeV/c.

The two factors so far described, the geometric factor and the potential factor when combined yield a momentum cut-off for both components of about 260 MeV/c.

Finally it is necessary to consider the ability of the projectile nucleus to absorb the energy $\hbar\omega$ and the momentum $\hbar q$. If the energy is absorbed by a single nucleon it will be very far off the energy shell. If it absorbs the full energy $\hbar\omega$ it will have a momentum $\sqrt{2m\hbar\omega}$. This however is very much larger than the momentum transferred which as we have seen is of the order of $\hbar\omega/c$, that is

$$\sqrt{2m\hbar\omega} \gg \hbar\omega/c$$

or

$$\sqrt{\hbar\omega/2mc^2} \ll 1 \tag{5.22}$$

This inequality is satisfied by the $\hbar\omega$ of interest, that $\hbar\omega < 260$ MeV. The absorbing nucleon must therefore interact with a second nucleon in the projectile. This absorption by two nucleons can proceed because it is then possible to conserve both momentum and energy. The momenta of the two nucleons will be opposite and nearly equal so that the total momentum is small but the total energy will be a sum of the energies of each nucleon.

The probability for two nucleon absorption will therefore depend critically upon the correlation length, r_c, the mean distance between the first nucleon and the second. From the uncertainty principle, the lifetime

of the nucleon absorbing the momentum and energy is of the the order of $(1/\omega)$. This nucleon moves with a velocity equal to $\sqrt{\frac{2}{m}\hbar\omega}$ and thus covers in the time $(1/\omega)$ the distance $\sqrt{\frac{2\hbar}{m\omega}}$. This distance must be of the order of or greater than r_c:

$$(2\hbar/m\omega)^{\frac{1}{2}} > r_c$$

or

$$\hbar\omega < 2\hbar^2/m r_c^2 \tag{5.23}$$

If we take r_c as $1/2\ \frac{\hbar}{m_\pi c}$, one half of the pion Compton wavelength, this inequality becomes

$$\hbar\omega < 165\ \text{MeV} \tag{5.24}$$

Combining this result with the geometrix and interaction potential gives a longitudinal momentum cut-off of 120 MeV/c, of the same order as the experimental value. It also implies a maximum value for the energy which can be transferred to the projectile equal to 120 MeV. This energy is split between the two absorbing nucleons so that the cut-off energy for one of these nucleons is approximately 60 MeV and the cut-off momentum of the order of 60 MeV/c.*

The low value of the momentum transferred ($\sim\hbar\omega/c$) indicates that the

---

*It has been suggested by A. Goldhaber that in addition to the two nucleon mechanism, there is the possibility of nucleon excitation to form a Δ. However the momentum change would then be of the order of 300 MeV/c. This combined with the other factors would yield a cut-off of 190 MeV/c which would be too large to explain the fragmentation data. However as Deutchmann and Brown pointed out, it could be an important mechanism for pion production.

angular distribution of the nucleons will be roughly isotropic. In the collision of the two nucleons as discussed above, their final linear momentum is $\hbar\omega/c$ so that their angular momentum $\ell\hbar$ is of the order of $(\hbar\omega/c)r_c$ so that

$$\ell \simeq \frac{\hbar\omega r_c}{\hbar c} \tag{5.25}$$

Inserting a maximum value for $\hbar\omega$ of 120 MeV and r_c = 0.7 fm yields

$$\ell \simeq 0.4 \tag{5.26}$$

demonstrating that for nearly all values of $\hbar\omega$ the angular distribution of the nucleon pair will be isotropic.*

These qualitative considerations provide a simple explanation of the projectile fragmentation as a consequence of the action of the "fringing field" of the target nucleus as it moves past the projectile. Our principal conclusion is that the process is essentially a low energy phenomenon. The energy of the nucleon pairs produced is predicted to have the observed order of magnitude. These nucleons will deposit energy within the projectile nucleus and by that means fragmenting it. The net maximum momentum which can be transferred is calculated to be of the experimental order of magnitude. A rough isotropy is also predicted. Energy dependence in the GeV/A range is weak since the energy occurs only in the geometric cut-off given by Eq. (5.19). The cut-off energy is changed by only a few percent when the heavy ion energy is changed from 2.1 GeV/A to 1.05 GeV/A as observed, since the dynamical conditions, Eq. (5.23) and the limits imposed by the nucleon-nucleon potential are energy independent in this range of energy. Finally it should be observed that none of the cut-off conditions depend upon the target nucleus. This

*Actual calculation shows in fact that this estimate is over-generous and that the maximum value of ℓ is considerably smaller than that given by Eq. (5.26).

does indicate that the widths of the momentum distribution of the fragments is independent of the target. It is obviously a necessary condition for showing that the branching ratios are target nucleus independent. However the quantitative calculation we shall report below shows that indeed the nucleon spectrum and therefore the projectile fragmentation is target independent.

We turn now to the formulation of the nuclear Weiszäcker-Williams method. We shall use the projectile frame of reference so that the incident system is the target nucleus. The derivation is similar to that used to develop the results for the Coulomb case. As in that case, the target nucleus is assumed to continue to move along a straight line along the incident direction. Secondly, it is assumed that the interaction is weak so that first order perturbation theory can be used. In the present case it is the long range part of the nuclear interaction, the "fringing field", which is assumed to be weak. Under these circumstances it can be shown that the total cross-section analogous to Eq. (5.17) is given by [29]

$$\sigma_T = (2\pi/\hbar)^2 \int \rho_\beta \, dE_\beta \, d\vec{k} \, d\omega \, |F_p(-\vec{k}, -\omega/v)|^2 |F_T(\vec{k}, \omega/v)|^2 \, \delta(\omega - \omega_{\beta i}) \tag{5.27}$$

where

$$F_T = (1/2\pi v) \tilde{V}(\vec{k}, \omega/v) \, \tilde{\rho}_T(-\vec{k}, -\omega/\gamma v) \tag{5.28}$$

and

$$F_p = \sum_f \langle \psi_\beta | e^{i\vec{q}\cdot\vec{\xi}_p} | \psi_i \rangle \qquad \vec{q} = (-\vec{k}, -\omega/v) \tag{5.29}$$

In these formulas, $\vec{k}$ gives the transverse momentum transfer and ω/v the longitudinal in units of $\hbar$; v is the velocity. The energy transfer is $\omega_{\beta i}$, with the projectile being excited to an energy E_β. The density of these levels is given by ρ_β. The target form factor, F_T, involves the Fourier transform

of the nucleon-nucleon potential $V(\vec{r})$:

$$\tilde{V}(\vec{\varkappa}) = \int \exp(-i\vec{\varkappa}\cdot\vec{r})\, V(\vec{r})\, d\vec{r}$$

The factor $\tilde{\rho}$ is related to the transform of the peripheral target density corrected for absorption as discussed above. Finally, the form factor F_p is just the matrix element of the Fourier component of the perturbation. Only a rough evaluation of the factors $\tilde{\rho}$ and F_p have been made. A quasi-deuteron model was used to evaluate the latter. This involves the only empirical parameter which has been used, namely the correlation length r_c. The results are shown in Fig. (5.7), (5.8) and (5.9). In Fig. (5.7) the upper curve provides the longitudinal part of the form factor $|F_T|^2$; the transverse part is given by Fig. (5.8). The lower curve in Fig. (5.7) contains the additional factor coming from $|F_p|^2$. The latter is exact in the limit of a large projectile radius. For finite radii it is in error at the small momentum end because of the lack of orthogonality of the crude representation used for ψ_β and ψ_i. A more precise calculation is needed, but the error should be small for momentum above $\hbar/R$ where R is the projectile radius. Fig. (5.9) gives the cross-section for a Ca target and an oxygen projectile as a function of r_c. It is clear that a reasonable value of r_c will yield the correct order of magnitude for the cross-section. A more severe test is the calculation of the branching ratio. Zabek [38] has obtained the results given in Table 5.2 where he has included the effect of single nucleon transfer as well as the process described above. The agreement is excellent.

Other applications of the nuclear Weiszäcker-Williams method are given in the second of the references in [28].

Table 5.2

Branching Ratios: Fragmentation of 2.1 GeV/nucleon ^{16}O

TARGET	Cu	Pb	Theory (r_c = 0.8 fm)
$\sigma(^{12}C)/\sigma_{TOT}$	0.105 ± 0.016	0.123 ± 0.024	0.128
$\sigma(^{11}C)/\sigma_{TOT}$	0.031 ± 0.003	0.036 ± 0.009	0.029
$\sigma(^{11}B)/\sigma_{TOT}$	0.041 ± 0.003	0.051 ± 0.006	0.040
$\sigma(^{10}B)/\sigma_{TOT}$	0.040 ± 0.006	0.034 ± 0.011	0.043

Figure Captions

Figure 1.1. (no caption)

Figure 2.1. Elastic scattering of 1.04 GeV protons by ^{208}Pb. The theoretical predictions for $\rho_n = \rho_p$ and $\rho_n \neq \rho_p$ are compared (from Ref. [7]).

Figure 2.2. Comparison of experiment with theoretical predictions for the elastic and inelastic scattering of 1.04 GeV protons by ^{208}Pb (from Ref. [7]).

Figure 2.3. The difference between the neutron and proton radii for the Calcium isotopes as obtained from the elastic scattering of 1 GeV protons and other hadrons (from Ref. [9]).

Figure 3.1. (no caption)

Figure 3.2. Decomposition of the imaginary part of the expectation value of the isobar-hole Hamiltonian. Γ is the free space isobar width (from Ref. [10]).

Figure 3.3. The energy dependence of the spreading width potential in the absence of a spin-orbit term (from Ref. [10]).

Figure 3.4. The energy dependence of the spreading width potential including the spin-orbit potential (from Ref. [11]).

Figure 3.5. The volume integral of the central part of single particle potentials. For a definition of U see text (from Ref. [11]).

Figure 3.6. The surface integral of the L-S potential (from Ref. [11]).

Figure 3.7. Absorption cross-section for π - ^{12}C as a function of the pion kinetic energy (from Ref. [11]).

Figure 3.8. Angular distribution for π - ^{12}C elastic scattering for indicated pion energies (from Ref. [11]).

Figure 3.9. Angular distribution for π - ^{12}C elastic scattering for indicated pion energies (from Ref. [11]).

Figure 3.10. Angular distribution for π - ^{12}C elastic scattering for indicated pion energies (from Ref. [11]).

Figure 3.11. π - ^{16}O elastic scattering at 114 and 240 MeV. Solid lines: spin orbit term included. Dashed lines: without spin-orbit term (from Ref. [11]).

Figure 3.12. π - ^{4}He elastic scattering at 220 and 260 MeV. For significance of solid and dashed lines, see caption for Fig. 3.11 (from Ref. [11]).

Figure 3.13. π - ^{12}C elastic scattering at 180 and 200 MeV. For significance of solid and dashed lines, see caption for Fig. 3.11 (from Ref. [11]).

Figure 4.1. The broken line gives the momentum of the Λ formed in the reaction Eq. (4.1). The solid line is the differential cross-section for the forward production of a pion in this reaction (from Ref. [16]).

Figure 4.2. Production of Λ hypernuclear states (from Ref. [21]).

Figure 4.3. Production of Σ hypernuclei (presented at the Jablona, Poland Conference, 1979).

Figure 4.4. Energy levels of ^{12}C (from Ref. [26]).

Figure 4.5. Angular distribution of pions in production of indicated hypernuclear states in ^{12}C (from Ref. [27]. Experimental data from Chrien, et al., Phys. Lett. 89B, 30 (1979)).

Figure 4.6. Angular distribution of pions in production of indicated hypernuclear states in ^{12}C (from Ref. [27]. Experimental data from Chrien, et al., Phys. Lett. 89B, 30 (1979),.

Figure 5.1. Energy dependence of ranges of Sc nuclei produced when protons of energy E_p are incident on a ^{238}U (from Ref. [30]).

Figure 5.2. Ratio of forward (F) to backward (B) production as a function of the incident proton energy E_p. The target is ^{238}U (from Ref. [30]).

Figure 5.3. Angular distribution of Flourine fragments produced by 28 GeV protons incident on Uranium (from Ref. [31]).

Figure 5.4. Angular dependence of the ratio of the multiplicity for the indicated target nuclei with the multiplicity for a hydrogen target (from Ref. [32]).

Figure 5.5. The longitudinal momentum distribution in the projectile frame of reference of the ^{10}Be fragments produced by the fragmentation of a ^{12}C projectile with an energy of 2.1 GeV/nucleon (from Ref. [34]).

Figure 5.6. Target averaged values of the dispersion σ of the longitudinal momentum distribution in the projectile frame. The plotted numeral gives the charge of the fragment. The projectile is ^{16}O with an energy of 2.1 GeV/nucleon. The solid line is a best fit using Eq. (5.4) (from Ref. [34]).

Figure 5.7. Longitudinal frequency spectrum. The lower curve gives the combined effect of the longitudinal frequency spectrum and the two nucleon absorption probability (from Ref. [29]).

Figure 5.8. Transverse momentum spectrum for a ^{40}Ca target in arbitrary units (from Ref. [29]).

Figure 5.9. The cross-section σ_{Ca} when the projectile energy is 2.1 GeV/n as a function of the correlation length Λ_c.

References

1. A.K. Kerman, H. McManus and R.M. Thaler, Ann. Phys. (N.Y.) 8, 551 (1959).
2. H. Feshbach, A. Gal and J. Hüfner, Ann. Phys. (N.Y.) 66, 20 (1971); E. Lambert and H. Feshbach, Ann. Phys. (N.Y.) 76, 80 (1973); J.J. Ullo and H. Feshbach, Ann. Phys. (N.Y.) 82, 156 (1974).
3. M.L. Goldberger and K.M. Watson, Collision Theory (New York: 1964).
4. R.J. Glauber, Lectures in Theoretical Physics (W.E. Britten, ed.), (New York: 1959) 1, 315.
5. C.J. Joachain, Quantum Collision Theory (Amsterdam: 1975), p. 591.
6. G. Takeda and K.M. Watson, Phys. Rev. 97, 1336 (1955).
7. E. Boridy and H. Feshbach, Phys. Lett. B 50, 433 (1974); Ann. Phys. (N.Y.) 109, 468 (1977).
8. J.W. Negele, Phys. Rev. C 1, 1260 (1970).
9. A. Chaumeaux, V. Layley and R. Schaeffer. Phys. Lett. B 72, 1 (1977).
10. M. Hirata, J.H. Koch, F. Lenz and E.J. Moniz, Ann Phys. (N.Y.) 120, 205 (1979); E.J. Moniz, Theoretical Methods in Medium Energy and Heavy Ion Physics (K. McVoy and W. Friedman, eds.) (New York: 1978), p. 603; E.J. Moniz, Nuclear Physics With Heavy Ions and Mesons (R. Balian, M. Rho and G. Ripka, eds.) (Amsterdam: 1978), p. 436.
11. *Y. Horikawa, N. Thies and F. Lenz, M.I.T. Center for Theoretical Physics* Preprint #844, March 1980.
12. L.S. Kisslinger and W.L. Wang, Phys. Lett. 30, 1071 (1973); Ann. Phys. (N.Y.) 99, 374 (1976).
13. H. Feshbach, Ann. Phys. (N.Y.) 5, 357 (1958); 19, 287 (1962); F.S. Levin and H. Feshbach, Reaction Dynamics (New York: 1973), p. 169.
14. H. Feshbach, A.K. Kerman, and R.H. Lemmer, Ann. Phys. (N.Y.) 41, 230 (1967).
15. P.M. Morse and H. Feshbach, Methods of Theoretical Physics (New York:

1953), p. 1155; R.R. Whitehead, A. Watt, B.J. Cole and I. Morrison, Advances in Nuclear Physics (M. Baranger and E. Vogt, eds.) (New York: 1977), Vol. 9.
16. A. Gal, Advances in Nuclear Physics (M. Baranger and E. Vogt, eds.) (New York: 1976), Vol. 8, p. 1.
17. G.C. Bonazzola, T. Bressani, R. Cister, E. Chiavassa, G. Pellacasou, A. Fainberg, O. Freschi, N. Mirfakhrai, A. Musso and G. Rinaudo, Phys. Lett. 53B, 297 (1974); Phys. Rev. Lett. 34, 683 (1975).
18. B. Povh, Reports on Progress in Physics 39, 824 (1976); Ann. Rev. Nucl. Part. Sci. 28, 1 (1978).
19. H. Feshbach and A.K. Kerman, Preludes in Theoretical Physics (A. deShalit, H. Feshbach and L. van Hove, eds.) (Amsterdam: 1965), p. 260; M.I. Podgoretsky, J.E.T.P. 44, 695 (1963).
21. *W. Brueckner, B. Granz, D. Ingham, K. Kilian, U. Lyman, J. Niewish, B. Pietrzyk, B. Povh, H.G. Ritter, and H. Schroeder, Phys. Lett. 62B, 481 (1976).*
22. P. Bertini, O. Bing, P. Berien, H. Catz, A. Chameaux, J.M. Durand, B. Mayer, W. Bruckner, M.A. Faessler, T.J. Ketel, K. Kilian, J. Niewisch, B. Pietrzyk, B. Povh, H.G. Ritter, U. Uhrmacher and A. Bouyssy, Phys. Lett. 90B, 375 (1980).
23. A. Gal and C.B. Dover, Phys. Rev. Lett. 44, 379 (1980).
24. R. Engelmann, et al., Phys. Lett. 21, 587 (1966).
25. *H. Feshbach, Proceedings of the Summer Study Meeting on Nuclear and Hypernuclear Physics with Kaon Beams (H. Palevsky, ed.) (New York: 1973), p. 185; H. Feshbach, Meson-Nuclear Physics - 1976 (P.D. Barnes, R.A. Eisenstein, L.S. Kisslinger, eds.) (New York: 1976), p. 521.*
26. R.H. Dalitz and A. Gal, Ann. Phys. (N.Y.) 116, 167 (1978).
27. C.B. Dover, A. Gal, G.E. Walker, and R.H. Dalitz, Phys. Lett. 89B, 26

(1979).

28. H. Feshbach, Nuclear Physics with Heavy Ions and Mesons (R. Balian, M. Rho, and G. Ripka, eds.) (Amsterdam: 1978), p. 375; H. Feshbach, First Workshop on Ultra-Relativistic Nuclear Collisions (Berkeley: 1979), p. 261.
29. H. Feshbach, Progress in Particle and Nuclear Physics 4, 451 (1980); H. Feshbach and M. Zabek, Ann. Phys. 107, 110 (1977).
30. ϕ. Scheidemann and N.T. Porile, Phys. Rev. C14, 1534 (1976).
31. L.M. Remsberg and D.G. Perry, Phys. Rev. Lett 35, 361 (1975).
32. W. Busza, Proc. High Energy Physics and Nuclear Structure (D.E. Nagle, A.S. Goldhaber, C.K. Hargrove, R.L. Burman, and B.G. Storm, eds.) (New York: 1975), p. 211; J.E. Elias, W. Busza, C. Halliwell, D. Luckey, L. Volta and C. Young, Phys. Rev. Lett. 41, 285 (1978).
33. P. Siemens and J. Rasmussen, to be published.
34. H.H. Heckman, D.E. Greiner, P.J. Lindstrom and F.S. Beiser, Phys. Rev. 28, 926 (1972); D.E. Greiner, P.J. Lindstrom, H.H. Heckman, B. Cork and F.S. Beiser, Phys. Rev. 35, 159 (1975).
35. H. Feshbach and K. Huang, Phys. Lett. 47B, 300 (1973).
36. A.S. Goldhaber, Phys. Lett. 53B, 306 (1974).
37. L.M.C. Dutton, Phys. Lett. 25B, 425 (1967); D.V. Bugg, D.C. Salter, G.H. Stafford, R.F. George, K.F. Riley, and M.R. Yearian, Phys. Rev. 164, 980 (1966).
38. M. Zabek, private communication.

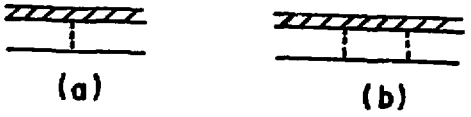

Fig. 1.1

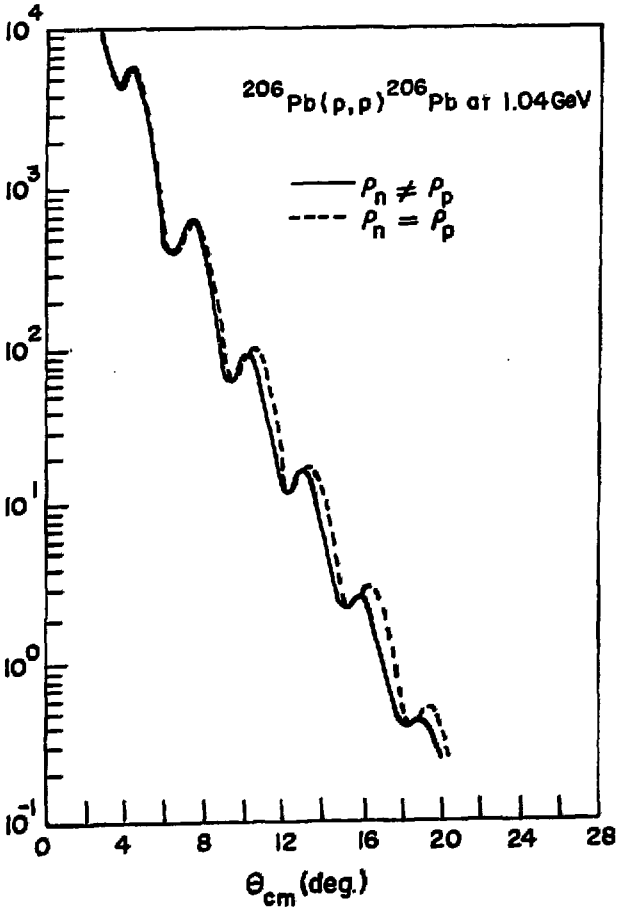
^{206}Pb(p,p)^{206}Pb at 1.04GeV
$\rho_n \neq \rho_p$
$\rho_n = \rho_p$
10^4
10^3
10^2
10^1
10^0
10^{-1}
0
4
8
12
16
20
24
28
θ_{cm}(deg.)

Fig. 2.1

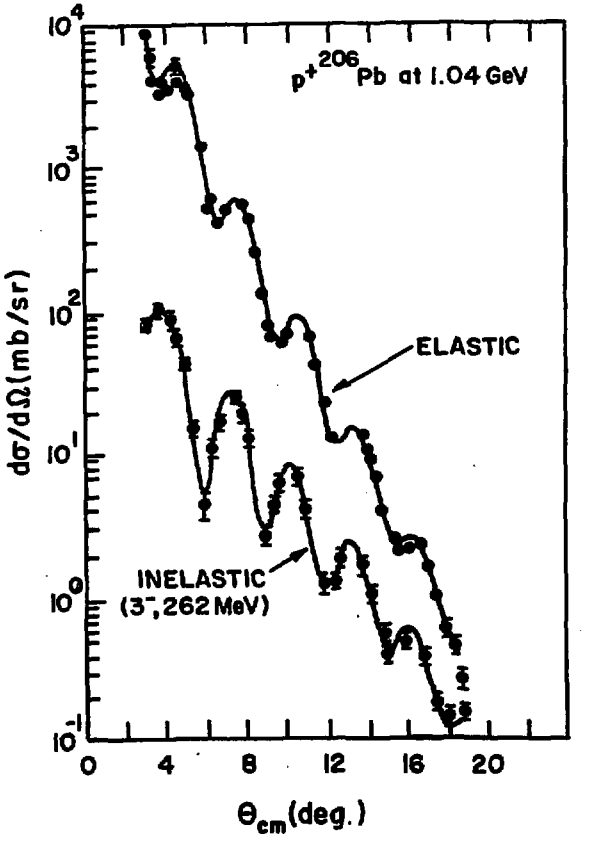
p+^{206}Pb at 1.04 GeV
ELASTIC
INELASTIC
(3$^-$,262 MeV)
$d\sigma/d\Omega$(mb/sr)
10^4
10^3
10^2
10^1
10^0
10^{-1}
0
4
8
12
16
20
θ_{cm}(deg.)

Fig. 2.2

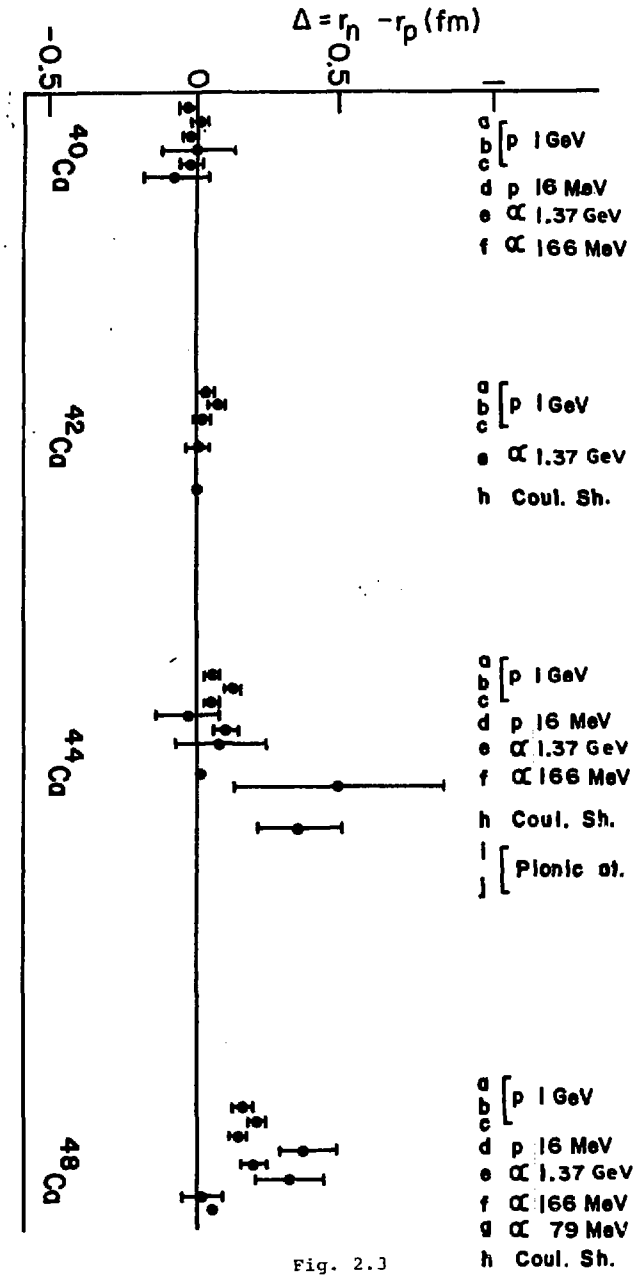
Δ = r_n − r_p (fm)
−0.5
0
0.5
40Ca
42Ca
44Ca
48Ca
a b c p 1 GeV
d p 16 MeV
e α 1.37 GeV
f α 166 MeV
a b c p 1 GeV
e α 1.37 GeV
h Coul. Sh.
a b c p 1 GeV
d p 16 MeV
e α 1.37 GeV
f α 166 MeV
h Coul. Sh.
i j Pionic at.
a b c p 1 GeV
d p 16 MeV
e α 1.37 GeV
f α 166 MeV
g α 79 MeV
h Coul. Sh.

Fig. 2.3

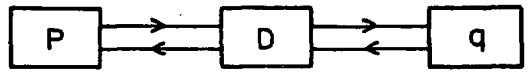
P
D
q

Fig. 3.1

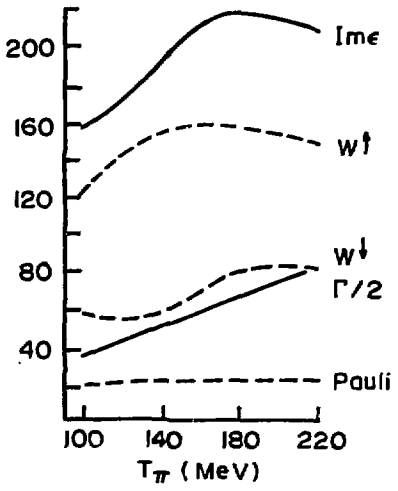
200
160
120
80
40
Imε
w↑
w↓
Γ/2
Pauli
100
140
180
220
T_π (MeV)

Fig. 3.2

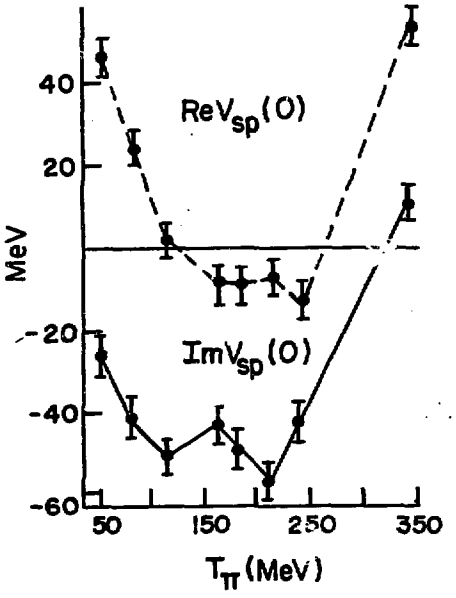
40
20
-20
-40
-60
MeV
$ReV_{sp}(0)$
$ImV_{sp}(0)$
50
150
250
350
T_π (MeV)

Fig. 3.3

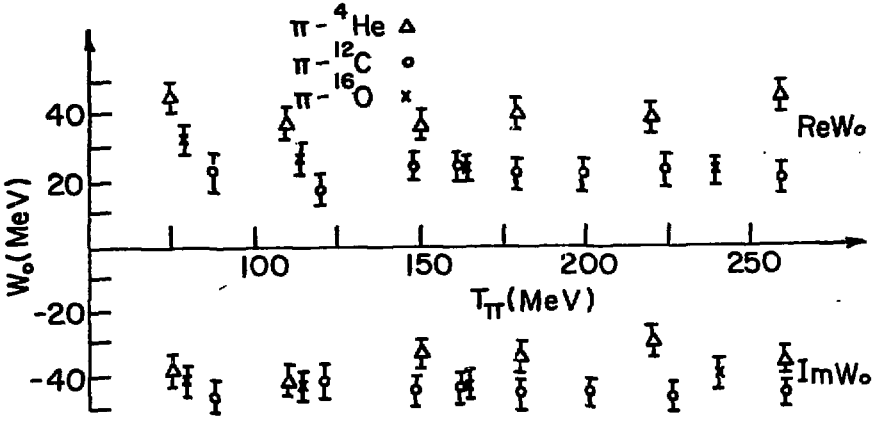
π - 4He
π - 12C
π - 16O
ReWo
ImWo
Wo(MeV)
40
20
-20
-40
100
150
200
250
Tπ(MeV)

Fig. 3.4

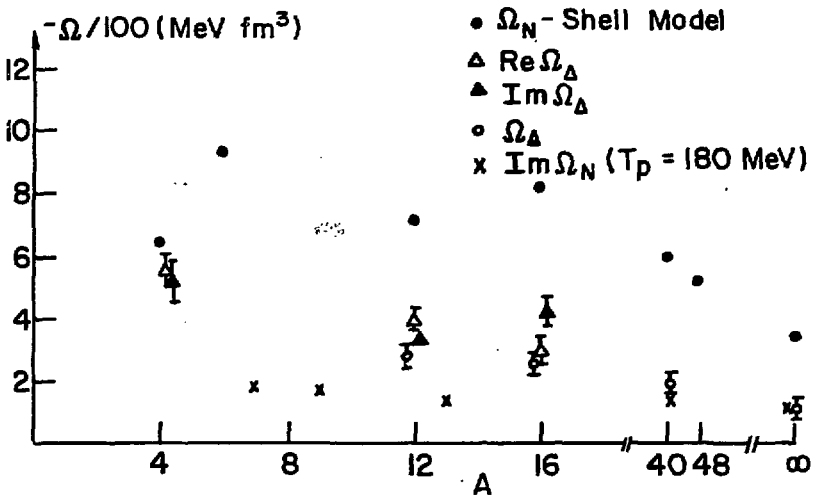
-Ω/100 (MeV fm3)
• ΩN - Shell Model
Δ Re ΩΔ
▲ Im ΩΔ
○ ΩΔ
x Im ΩN (Tp = 180 MeV)
12
10
8
6
4
2
4
8
12
16
40
48
∞
A

Fig. 3.5

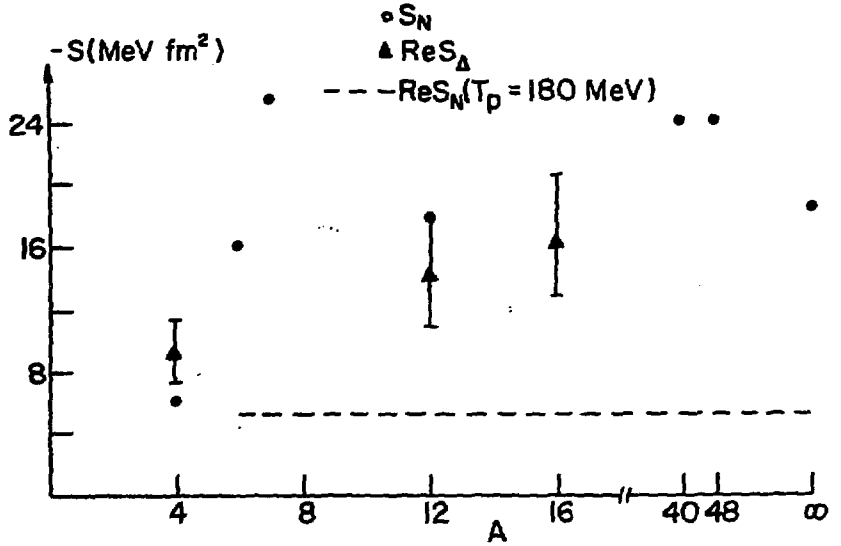
-S(MeV fm²)
∘ S_N
▲ ReS_Δ
- - - ReS_N(T_p = 180 MeV)
24
16
8
4
8
12
16
40
48
∞
A

Fig. 3.6

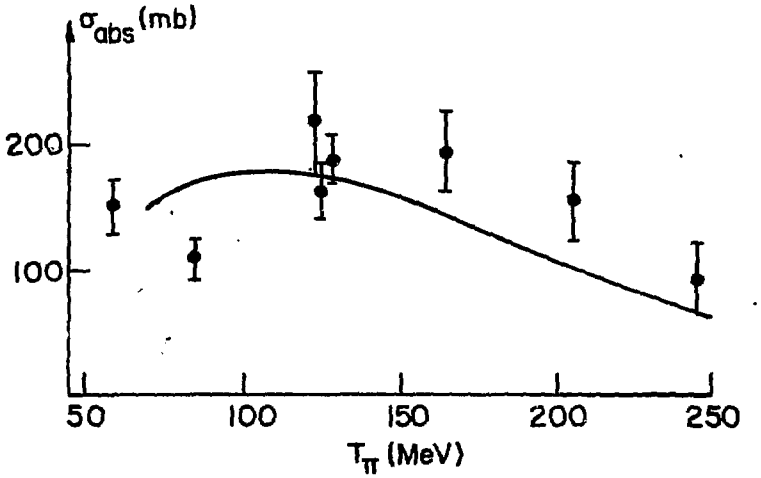
σ_abs (mb)
200
100
50
100
150
200
250
T_π (MeV)

Fig. 3.7

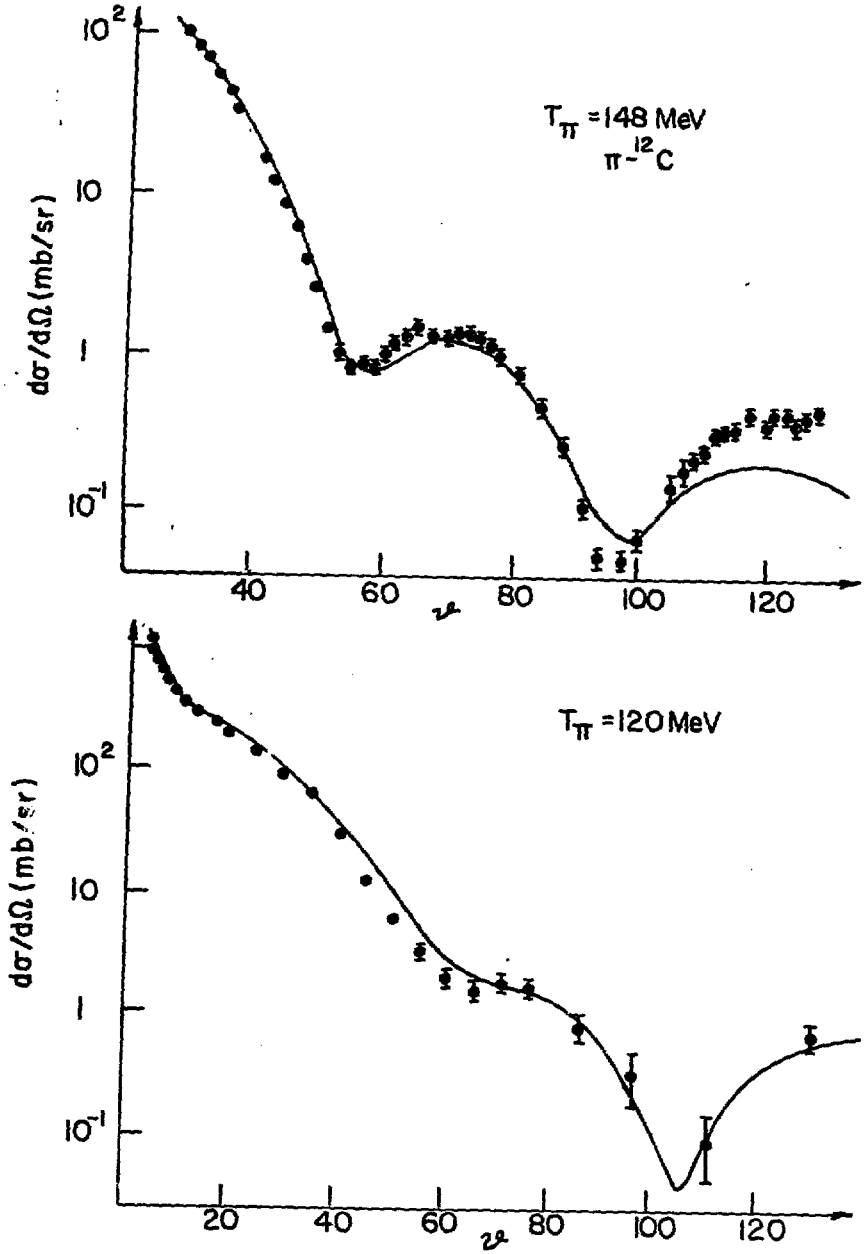
T_π = 148 MeV
$\pi^- - {}^{12}C$
$d\sigma/d\Omega$ (mb/sr)
10^2
10
1
10^{-1}
40
60
80
100
120
ϑ
T_π = 120 MeV
$d\sigma/d\Omega$ (mb/sr)
10^2
10
1
10^{-1}
20
40
60
80
100
120
ϑ

Fig. 3.8

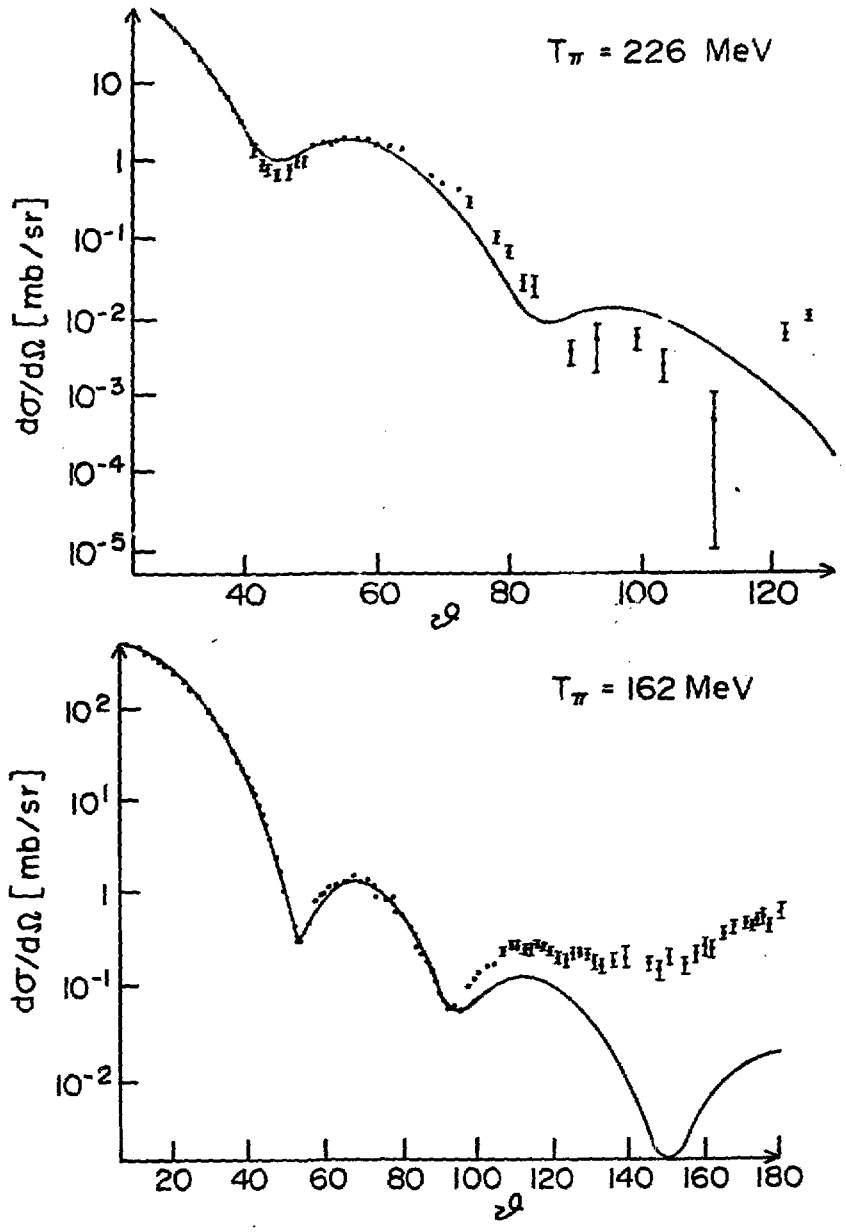
T_π = 226 MeV
$d\sigma/d\Omega$ [mb/sr]
10
1
10^{-1}
10^{-2}
10^{-3}
10^{-4}
10^{-5}
40
60
80
100
120
ϑ
T_π = 162 MeV
$d\sigma/d\Omega$ [mb/sr]
10^2
10^1
1
10^{-1}
10^{-2}
20
40
60
80
100
120
140
160
180
ϑ

Fig. 3.9

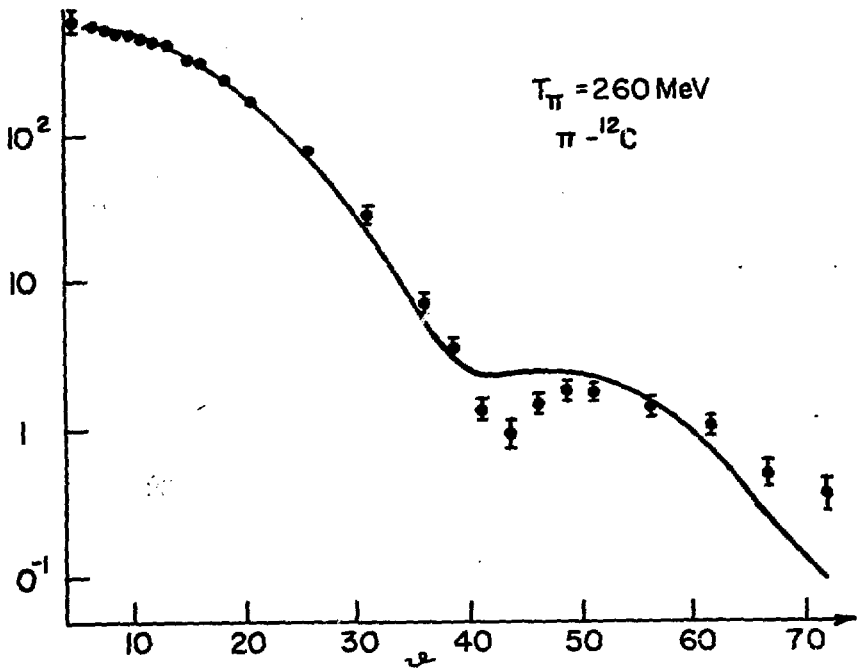

Fig. 3.10

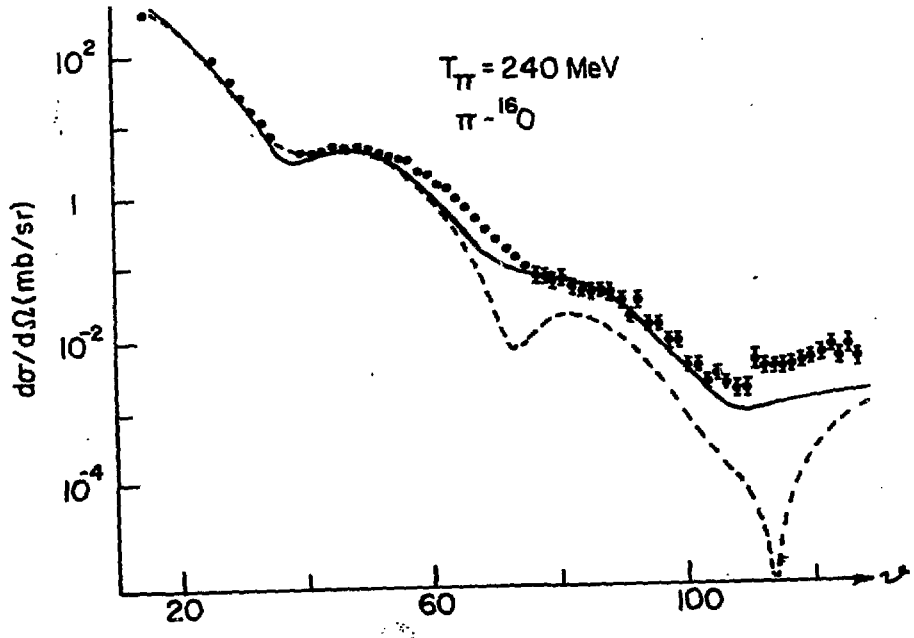

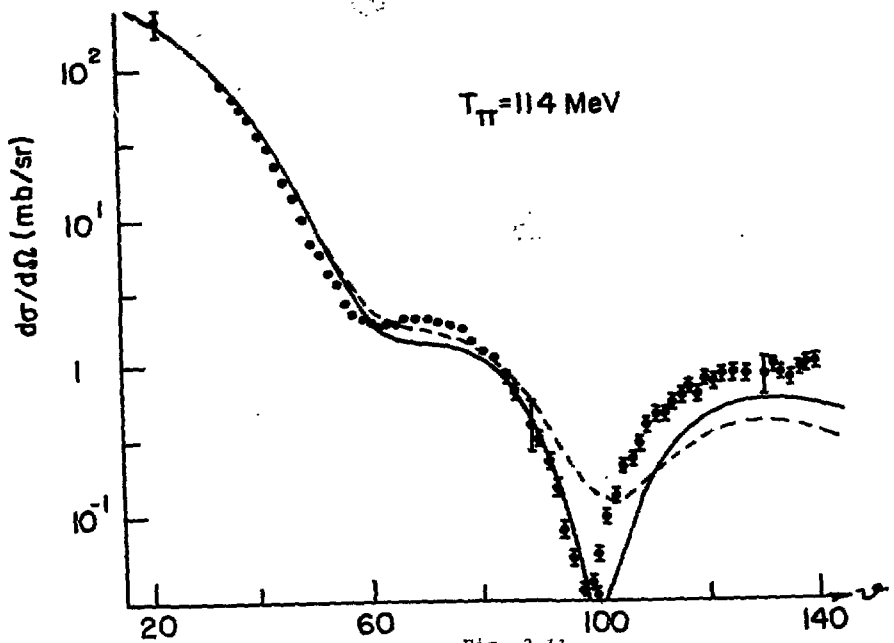

Fig. 3.11

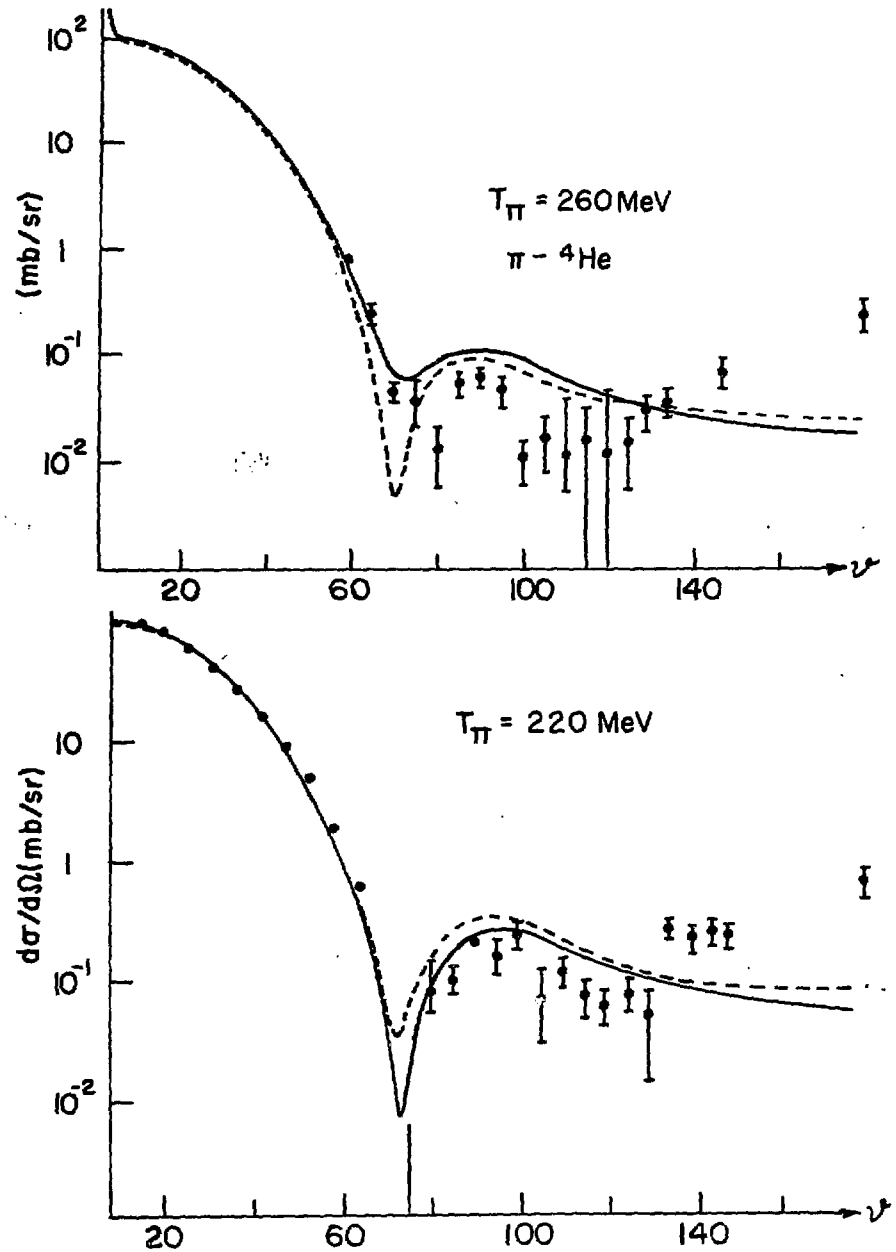

Fig. 3.12

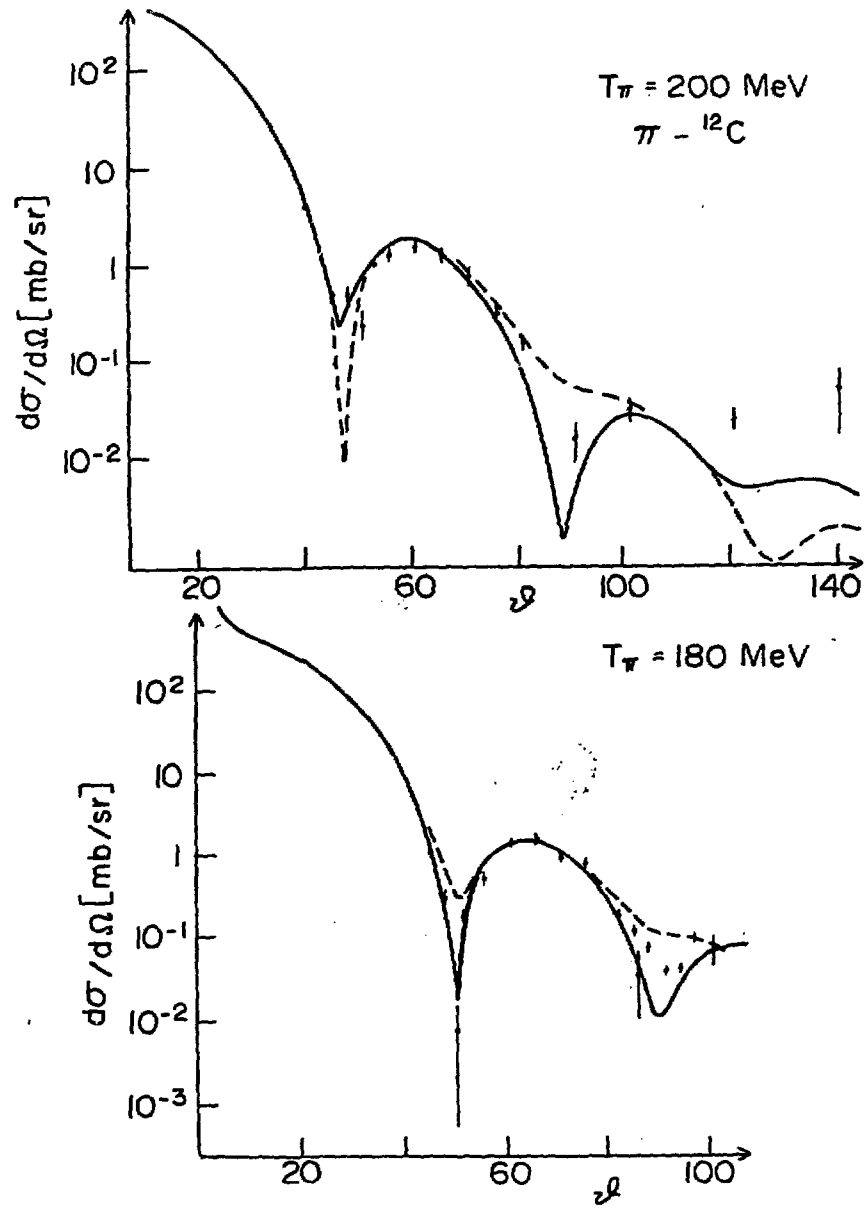

Fig. 3.13

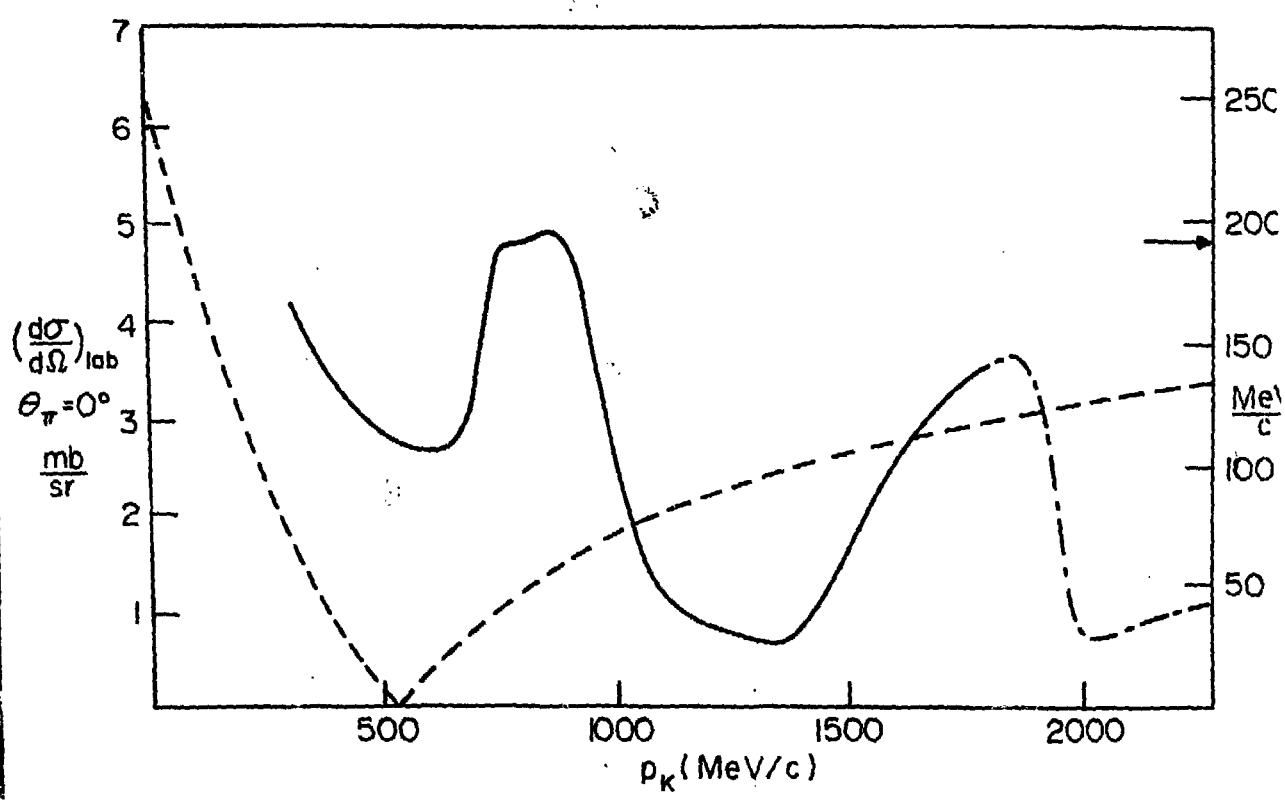
$\left(\frac{d\sigma}{d\Omega}\right)_{lab}$
$\theta_\pi = 0°$
$\frac{mb}{sr}$
p_K (MeV/c)
MeV/c

Fig. 4.1

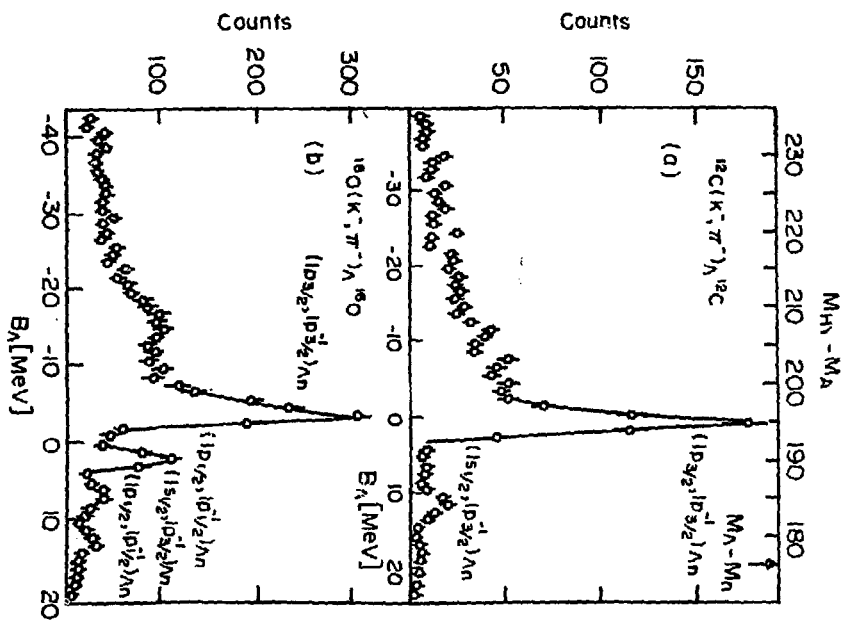
Counts
$M_{H\Lambda} - M_A$
$^{12}C(K^-,\pi^-)_\Lambda{}^{12}C$
(a)
$(1p_{3/2},1p^{-1}_{3/2})_{\Lambda n}$
$M_\Lambda - M_n$
$(1s_{1/2},1p^{-1}_{3/2})_{\Lambda n}$
$^{16}O(K^-,\pi^-)_\Lambda{}^{16}O$
(b)
$(1p_{3/2},1p^{-1}_{5/2})_{\Lambda n}$
$(1p_{1/2},1p^{-1}_{1/2})_{\Lambda n}$
$(1s_{1/2},1p^{-1}_{3/2})_{\Lambda n}$
$(1p_{1/2},1p^{-1}_{1/2})_{\Lambda n}$
B_Λ[MeV]

Fig. 4.2

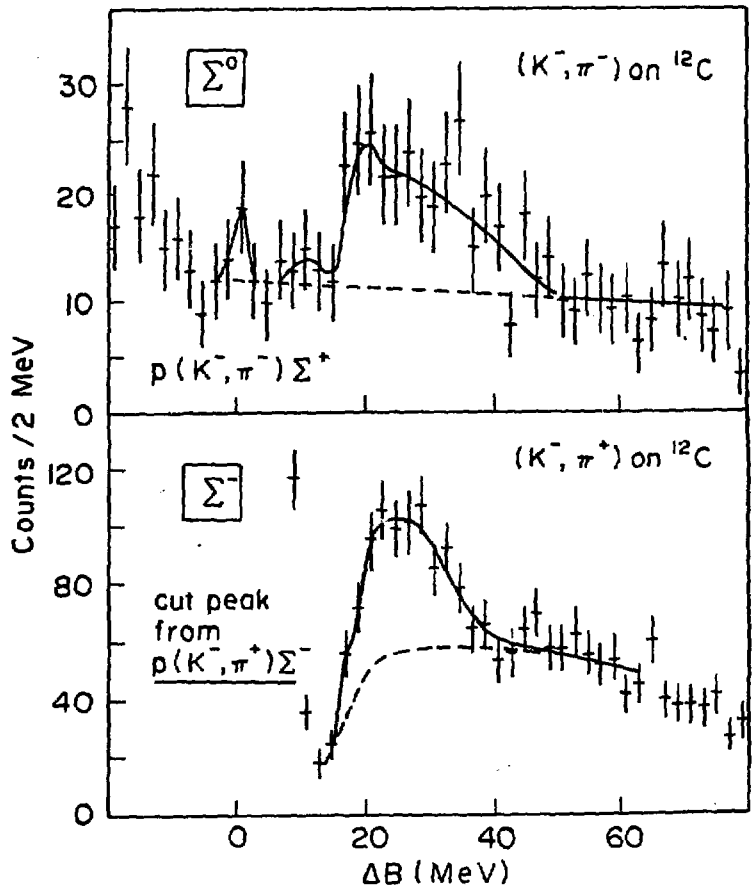
Σ⁰
(K⁻,π⁻) on ¹²C
p(K⁻,π⁻)Σ⁺
Σ⁻
(K⁻,π⁺) on ¹²C
cut peak
from
p(K⁻,π⁺)Σ⁻
Counts /2 MeV
ΔB (MeV)
0
10
20
30
40
60
80
120

Fig. 4.3

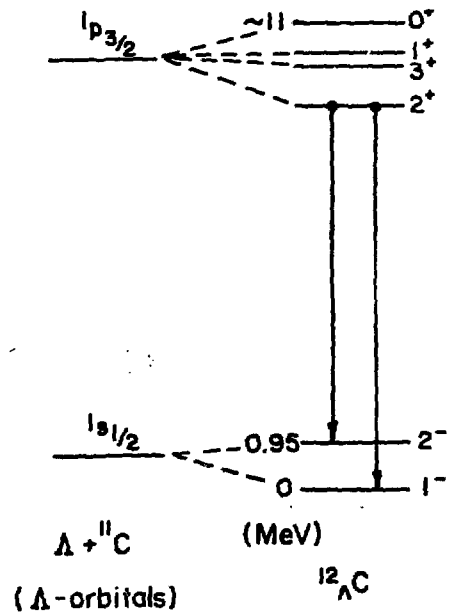
1p3/2
~11
0⁺
1⁺
3⁺
2⁺
1s1/2
0.95
2⁻
0
1⁻
Λ + ¹¹C
(MeV)
(Λ-orbitals)
¹²ΛC

Fig. 4.4

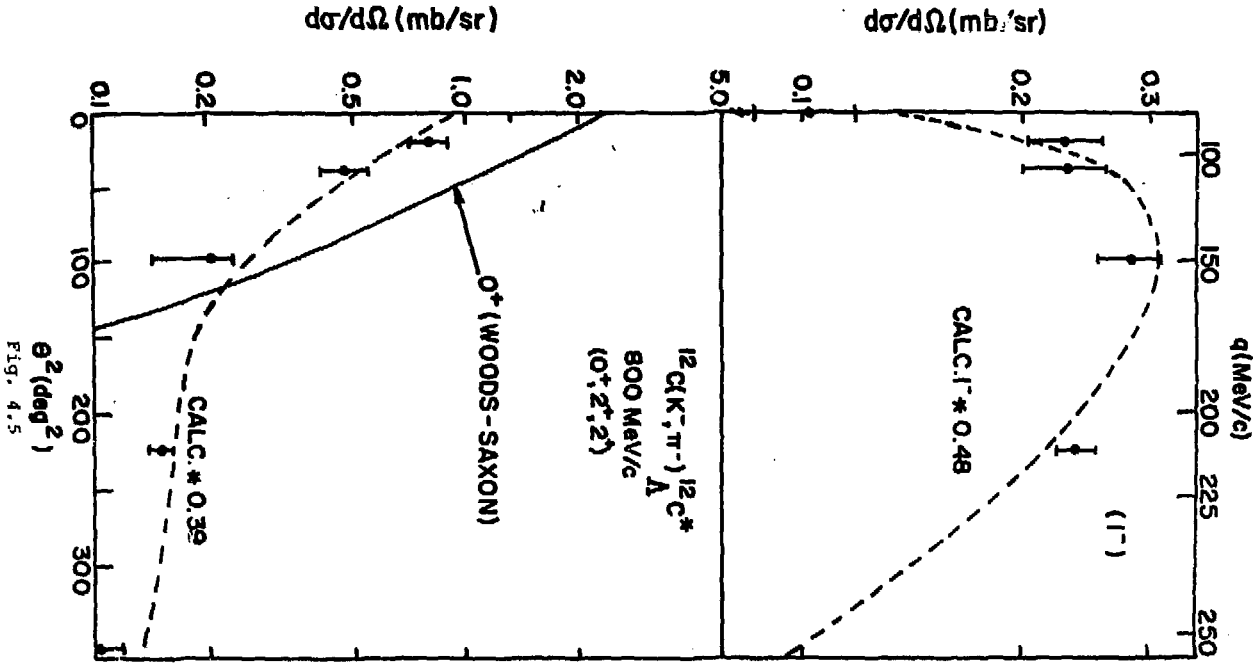
dσ/dΩ (mb/sr)
dσ/dΩ(mb/sr)
q(MeV/c)
0.1
0.2
0.5
1.0
2.0
5.0
0.1
0.2
0.3
100
150
200
225
250
0
100
200
300
θ²(deg²)
CALC.* 0.39
0⁺(WOODS-SAXON)
¹²C(K⁻,π⁻)¹²ΛC*
800 MeV/c
(0⁺,2⁺,2⁺)
CALC.1⁻ * 0.48
(1⁻)

Fig. 4.5

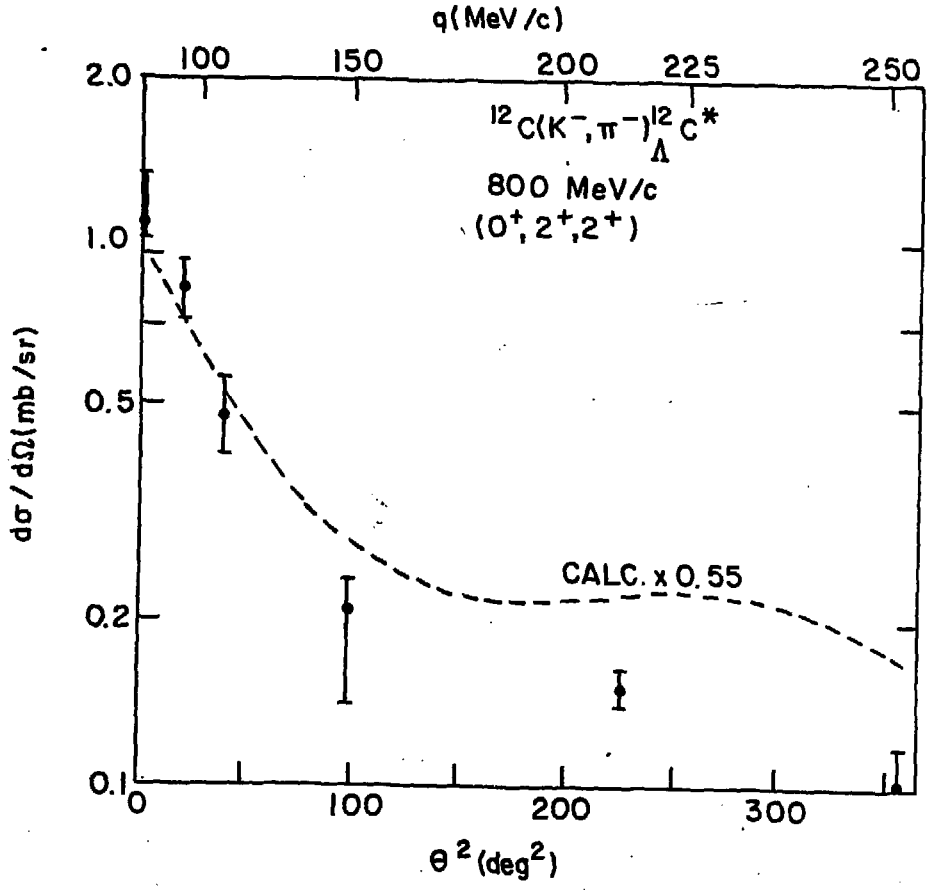
q(MeV/c)
100
150
200
225
250
2.0
1.0
0.5
0.2
0.1
dσ/dΩ(mb/sr)
¹²C(K⁻,π⁻)¹²ΛC*
800 MeV/c
(0⁺,2⁺,2⁺)
CALC. x 0.55
0
100
200
300
θ²(deg²)

Fig. 4.6

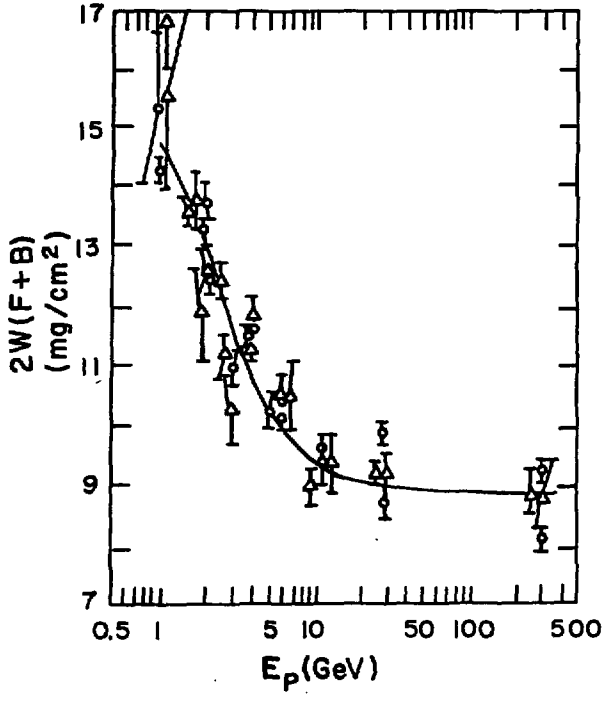
17
15
13
11
9
7
2W(F+B)
(mg/cm²)
0.5
1
5
10
50
100
500
Ep(GeV)

Fig. 5.1

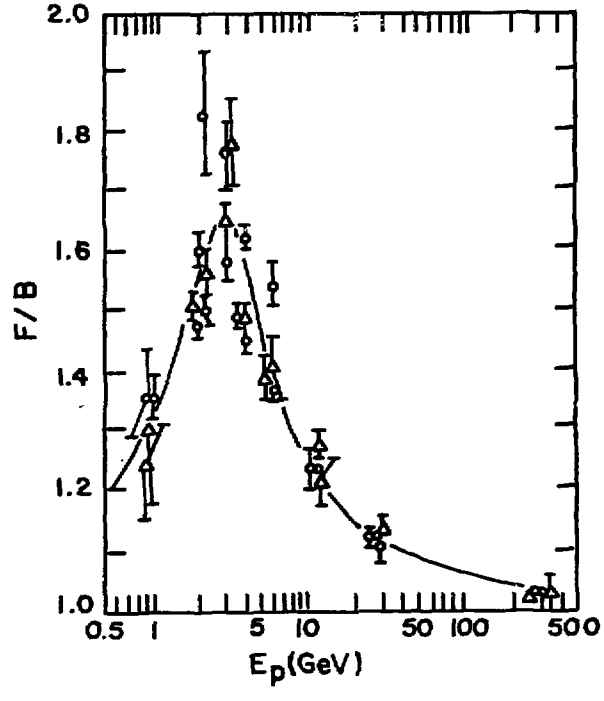
2.0
1.8
1.6
1.4
1.2
1.0
F/B
0.5
1
5
10
50
100
500
Ep(GeV)

Fig. 5.2

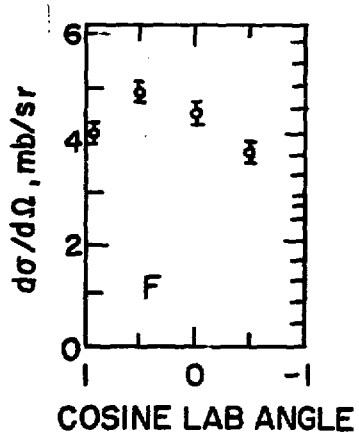
dσ/dΩ, mb/sr
6
4
2
0
F
1
0
-1
COSINE LAB ANGLE

Fig. 5.3

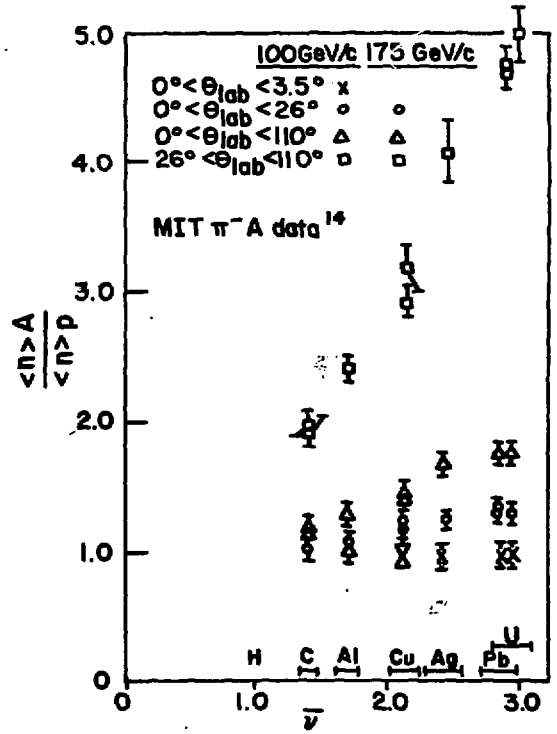
100GeV/c 175 GeV/c
0°<θlab<3.5° x
0°<θlab<26° o
0°<θlab<110° Δ
26°<θlab<110° □
MIT π⁻A data 14
<n>A / <n>p
5.0
4.0
3.0
2.0
1.0
0
H
C
Al
Cu
Ag
Pb
U
0
1.0
2.0
3.0
ν̄

Fig. 5.4

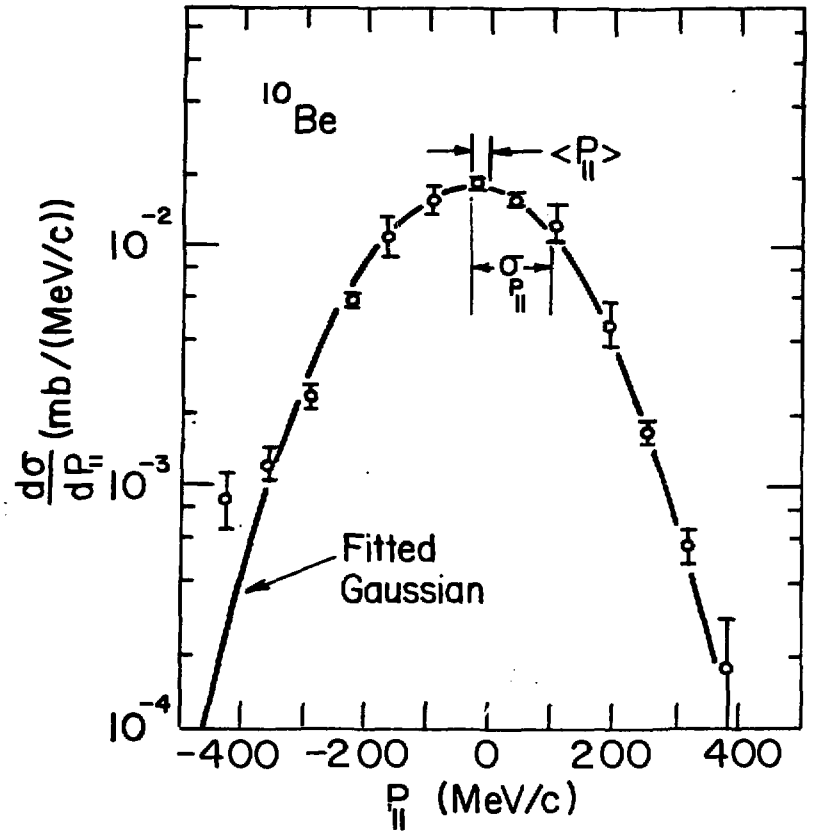
^{10}Be
$\langle P_{\parallel} \rangle$
$\sigma_{P_{\parallel}}$
Fitted Gaussian
$\frac{d\sigma}{dP_{\parallel}}$ (mb/(MeV/c))
10^{-2}
10^{-3}
10^{-4}
-400 -200 0 200 400
$P_{\parallel}$ (MeV/c)

Fig. 5.5

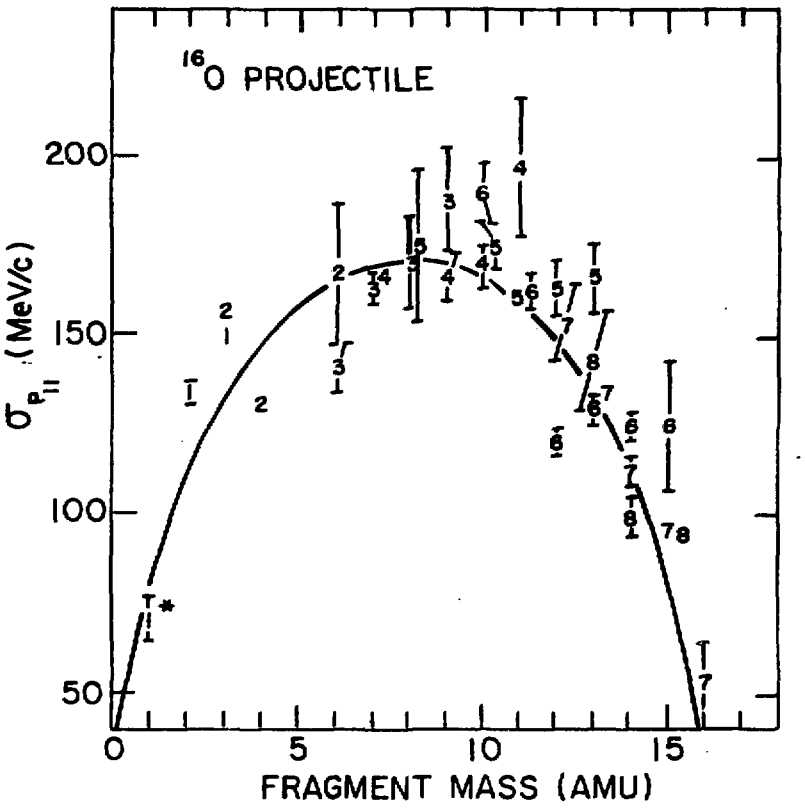
^{16}O PROJECTILE
$\sigma_{P_{\parallel}}$ (MeV/c)
200
150
100
50
0 5 10 15
FRAGMENT MASS (AMU)

Fig. 5.6

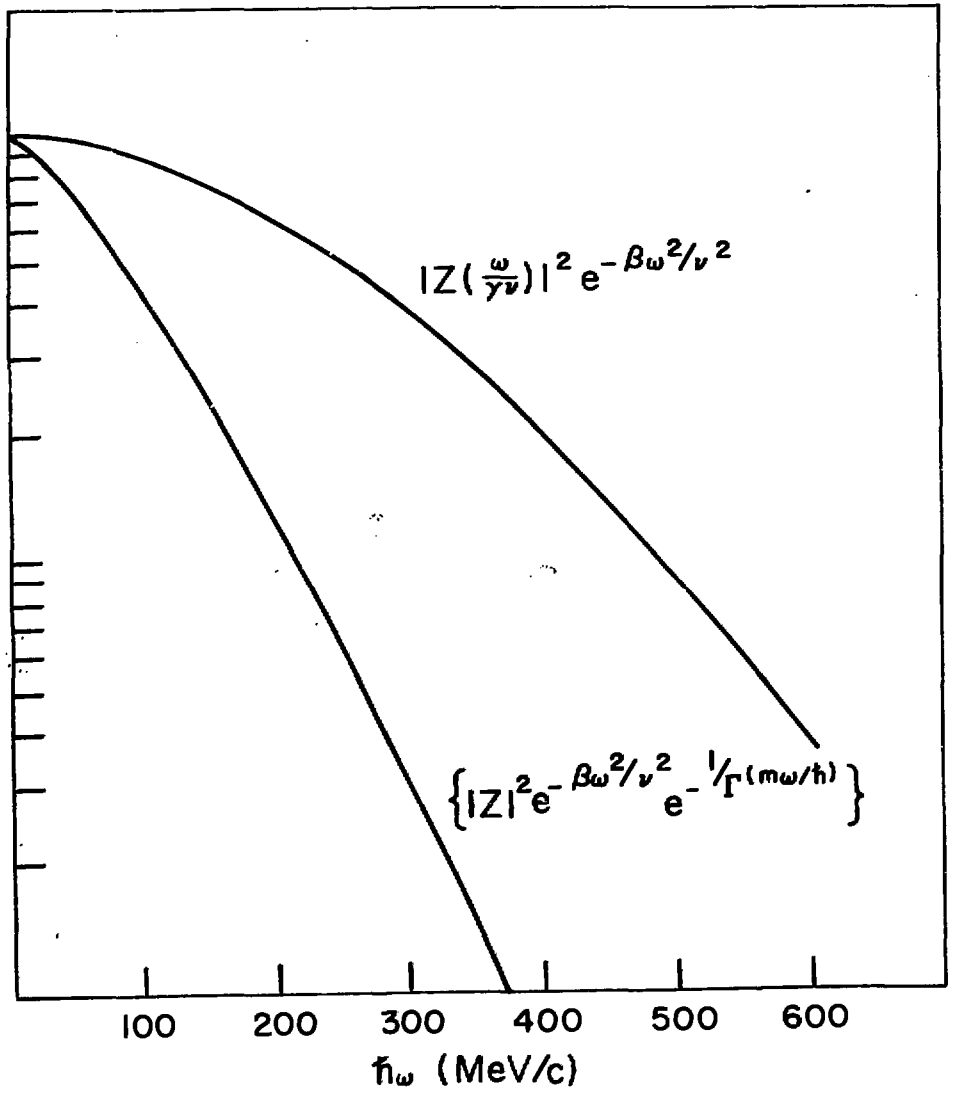
$|Z(\frac{\omega}{\gamma v})|^2 e^{-\beta\omega^2/v^2}$
$\{|Z|^2 e^{-\beta\omega^2/v^2} e^{-1/\Gamma(m\omega/\hbar)}\}$
100
200
300
400
500
600
$\hbar\omega$ (MeV/c)

Fig. 5.7

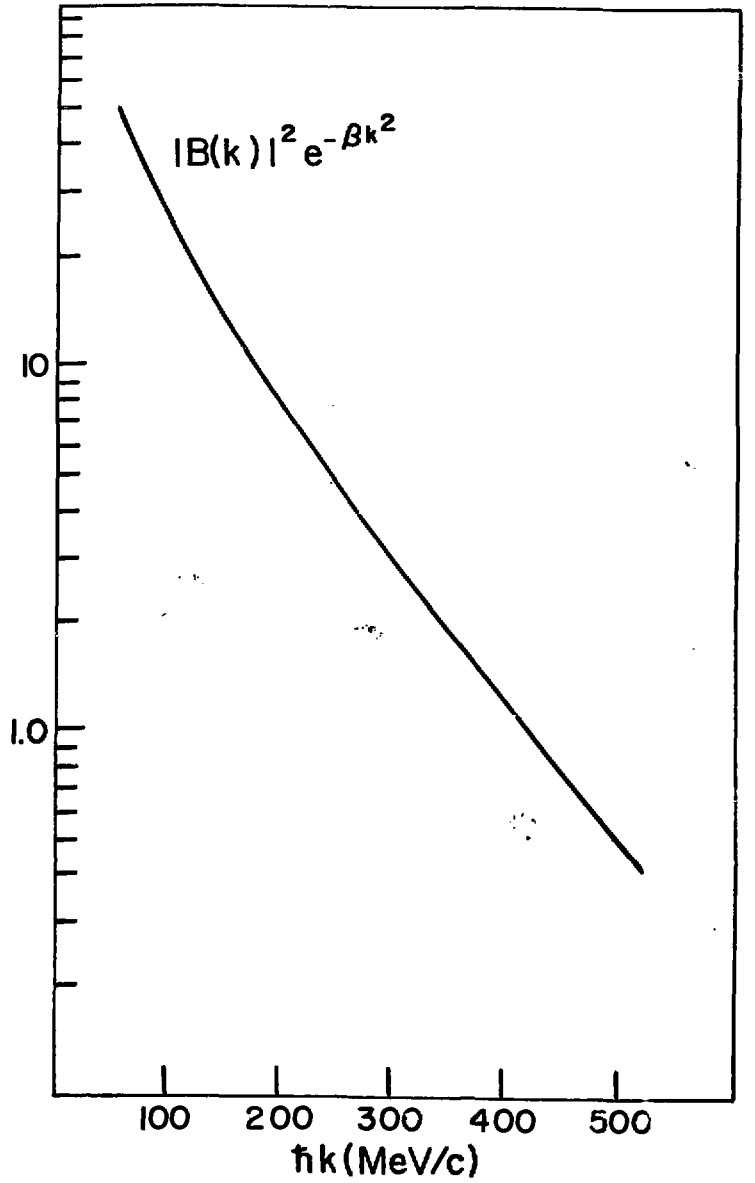
$|B(k)|^2 e^{-\beta k^2}$
10
1.0
100
200
300
400
500
$\hbar k$ (MeV/c)

Fig. 5.8

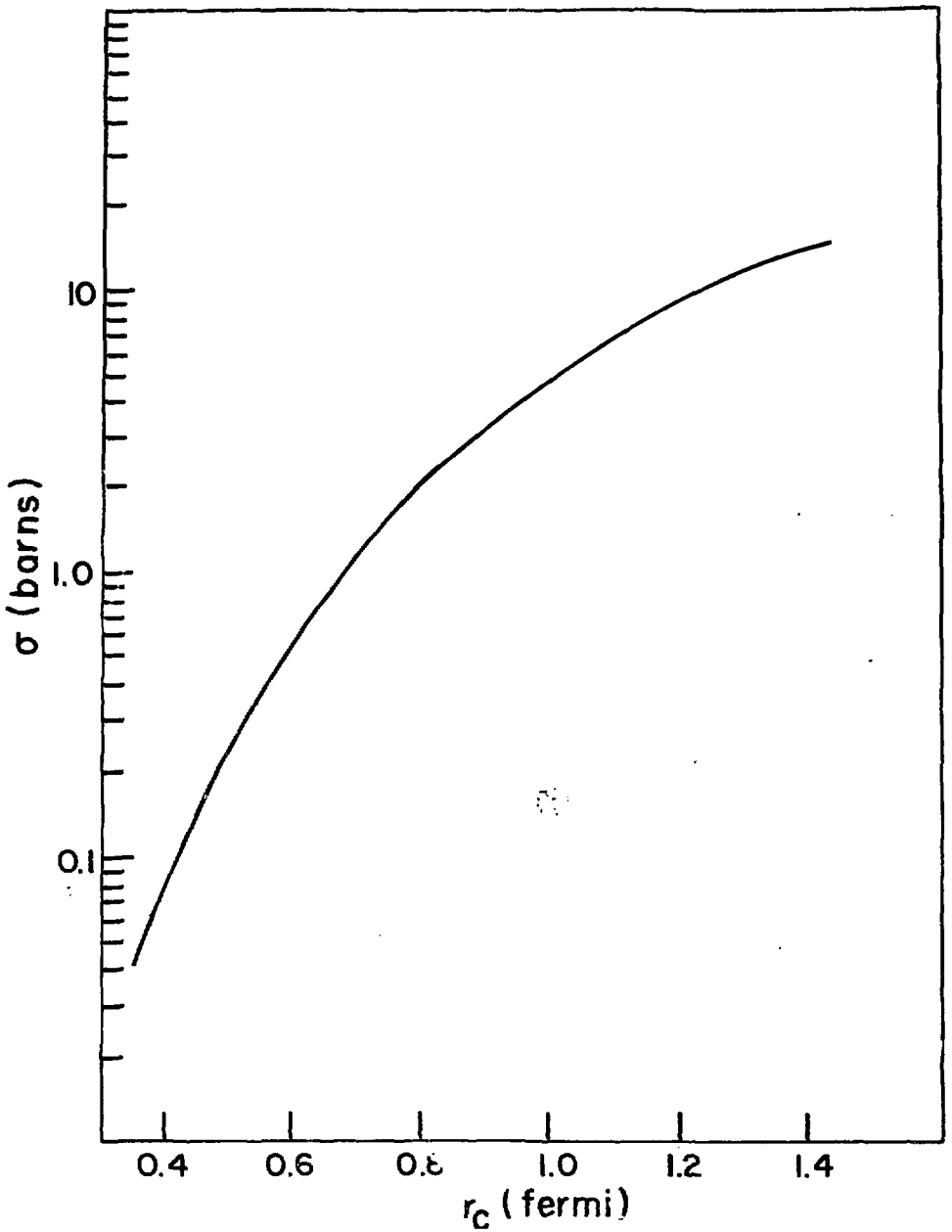

Fig. 5.9